

Blood-brain barrier permeability following intracerebral hemorrhage is related to local ion
dyshomeostasis

By

Colby Nadeau

A thesis submitted in partial fulfillment of the requirement for the degree of

Master of Science

Department of Psychology

University of Alberta

© Colby Nadeau, 2017

ABSTRACT

Background:

Increased blood-brain barrier (BBB) permeability is seen after intracerebral hemorrhage (ICH). Following ICH, BBB dysfunction occurs due to direct (*e.g.* mechanical damage) and indirect (*e.g.* inflammation) injury. Damage to the BBB prevents maintenance of brain homeostasis. This thesis seeks to elucidate the time course of BBB permeability after ICH and investigate its relationship to local ion dyshomeostasis using novel imaging techniques.

Methods:

Bacterial collagenase was used to cause a striatal hemorrhage in rats. In experiment 1, animals were euthanized at days 3, 7, and 14 post-ICH following injection of Evans Blue dye to measure BBB permeability. In experiment 2, animals were euthanized at day 3 post-ICH after injection with a gadolinium-based contrast agent. A novel *in situ* biospectroscopic imaging technique was used to spatially assess changes in iron, chlorine, potassium, manganese, zinc, calcium, and copper in relation to BBB permeability.

Results:

After stroke, BBB permeability was significantly elevated at day 3 and decreased over time (time main effect; $P < 0.001$). At day 3 and day 7, BBB permeability was significantly elevated in the IPSI hemisphere as compared to SHAM samples ($P < 0.001$; $P < 0.05$, respectively). Contralateral BBB permeability did not differ between experimental groups at any survival time ($P > 0.05$). A subset of animals displayed BBB hyperpermeability (*i.e.* greater than

maximum SHAM levels) at all times sampled. Chloride, iron, potassium, and manganese dyshomeostasis occurred in the hematoma ($P < 0.001$). Chloride, iron, and potassium levels normalized with distance into the perihematoma zone (distance main effect; $P < 0.001$, $P < 0.001$, $P < 0.001$, respectively). Elevated gadolinium levels were found in the hematoma ($P < 0.05$) and the perihematoma zone (distance main effect; $P < 0.001$). There was a relationship between gadolinium levels and ion dyshomeostasis in the perihematoma, but not hematoma, zone.

Conclusions:

After experimental ICH, BBB permeability is elevated acutely, and BBB dysfunction may persist for two weeks. A subset of animals display hyperpermeability at days 3, 7, and 14 after ICH. This elevated permeability may indicate the presence of cerebral microbleeds or angiogenesis. Furthermore, ion dyshomeostasis and BBB dysfunction occur in the perihematoma zone three days after ICH. Future work should directly assess the contribution of BBB disruption to ion dyshomeostasis and its impact on functional outcome.

PREFACE

This thesis is an original work and received research ethics approval from the University of Alberta Animal Care and Use Committee for Biosciences, Project AUP960.

Chapter 2 of this thesis is in preparation for publication as Nadeau CA, Dietrich K, Wilkinson CM, Nichol H, and Colbourne F, "Acute blood-brain barrier injury is associated with ion dyshomeostasis but not cerebral microbleeds." Nadeau CA was responsible for concept formation, data collection, data analysis, and manuscript composition. Dietrich K assisted with data collection and manuscript composition for experiment 3 (not included). Wilkinson CM assisted with data collection for experiments 1, 2, and 3. Nichol H provided methodological advice and refinement. Colbourne F was the supervisory author and was involved with concept formation and manuscript composition.

DEDICATION

This thesis is dedicated to my parents, Suzanne and Donald Nadeau.

ACKNOWLEDGEMENTS

First and foremost, I would like to thank my supervisor, Dr. Fred Colbourne, for his guidance, for his patience, and for allowing me the independence to grow as a researcher and as a person. This project would not have been possible without his knowledge, advice, and encouragement. Thank you to my committee members, Dr. Kyle Mathewson and Dr. Ian Winship, for their time, commitment, and valuable feedback. I would also like to thank my labmates Ana Klahr, Shannon Wowk, Michael Williamson, and Kristen Dietrich for taking the time out of their busy schedules to train me. I would also like to thank them, along with Cassandra Wilkinson, Jasmine Aziz, and Lane Liddle, for their support, teamwork, and flexible schedules.

I could not have done this without the help of my parents, Sue and Don, and my siblings, Austin and Haley. To my family, I am forever grateful for your love and support. I would be remiss if I did not express my deep appreciation for my partner, Jamie Dowell. Thank you for your enduring patience and positivity, for your insights, and for always keeping me steady when I am spinning.

I would like to thank the Heart and Stroke Foundation, the Canadian Institutes of Health Research, and the Department of Psychology at the University of Alberta for supporting this research.

TABLE OF CONTENTS

| | |
|---|----|
| CHAPTER 1..... | 1 |
| 1.1 Introduction..... | 1 |
| 1.2 Stroke..... | 1 |
| 1.2.1 Epidemiology..... | 1 |
| 1.2.2 Intracerebral hemorrhage..... | 4 |
| 1.2.2.1 Clinical manifestation..... | 5 |
| 1.2.2.2 Risk factors..... | 6 |
| 1.2.3 Rodent models of intracerebral hemorrhage..... | 7 |
| 1.2.4 Pathophysiology of intracerebral hemorrhage..... | 9 |
| 1.2.4.1 Primary damage..... | 10 |
| 1.2.4.2 Secondary damage..... | 11 |
| 1.2.4.2.1 Thrombin..... | 11 |
| 1.2.4.2.2 Hematoma resolution and blood cytotoxicity..... | 12 |
| 1.3 Blood-brain barrier dysfunction following intracerebral hemorrhage..... | 14 |
| 1.3.1 Blood-brain barrier physiology..... | 14 |
| 1.3.1.1 Function..... | 14 |
| 1.3.1.2 Structure..... | 15 |
| 1.3.2 Blood-brain barrier dysfunction in intracerebral hemorrhage patients..... | 16 |
| 1.3.3 Monitoring blood-brain barrier permeability..... | 17 |
| 1.3.4 Pathophysiology..... | 18 |
| 1.3.4.1 Inflammation..... | 19 |
| 1.3.4.1.1 Vascular integrity..... | 20 |
| 1.3.4.2 Edema..... | 21 |
| 1.3.4.3 Angiogenesis..... | 22 |
| 1.3.4.4 Ion dyshomeostasis..... | 23 |
| 1.3.4.4.1 Iron dyshomeostasis..... | 24 |
| 1.3.4.4.1.1 Oxidative stress..... | 26 |
| 1.3.4.4.2 Chloride dyshomeostasis..... | 27 |
| 1.4 Purpose..... | 28 |
| CHAPTER 2..... | 30 |
| 2.1 Introduction..... | 30 |
| 2.2 Materials and methods..... | 34 |
| 2.2.1 Subjects..... | 34 |
| 2.2.2 Experiment 1..... | 35 |
| 2.2.3 Experiment 2..... | 36 |
| 2.2.4 Statistical analysis..... | 39 |
| 2.3 Results..... | 39 |
| 2.4 Discussion..... | 43 |
| 2.5 Conclusions..... | 50 |

CHAPTER 3..... 51

- 3.1 Primary findings..... 51
- 3.2 Blood-brain barrier permeability is highest at day 3 and decreases thereafter.. 51
- 3.3 Blood-brain barrier injury varies between subjects and time..... 53
- 3.4 Acute ion dyshomeostasis occurs after intracerebral hemorrhage..... 54
- 3.5 Limitations..... 59
- 3.6 Future directions..... 61
- 3.7 Conclusions..... 62

Bibliography..... 63

Tables..... 77

Figures..... 80

LIST OF TABLES

Table 1-1. Comparison of the two most commonly used intracerebral hemorrhage models, including model characteristics and clinical relevance.

Table 2-1. Relationship (Pearson's rho) between Gd concentration and Ca, Cu, Cl, Fe, K, Mn, and Zn concentration in the hematoma and perihematoma zone at day 3 post-ICH. Bolded p -values indicate $p < 0.05$.

Table 2-2. Relationship (Pearson's rho) between Gd concentration and Fe, Cl, and K concentration every 180 μm into the perihematoma zone at day 3 post-ICH. Bolded p -values indicate $p < 0.05$.

LIST OF FIGURES

Figure 1-1. Blood-brain barrier structure. From Armin Kübelbeck (https://commons.wikimedia.org/wiki/File:Blood_vessels_brain_english.jpg), “Blood vessels brain English”, <https://creativecommons.org/licenses/by/3.0/legalcode>.

Figure 1-2. Fenton’s Reaction.

Figure 2-1. Evans Blue extravasation at day 3 was significantly higher than days 7, 14, and SHAM in the IPSI hemisphere. Significant elevations persisted to day 7. There were no differences in Evans Blue extravasation in the CONTRA hemisphere (A). High variability was observed at all times measured (B). A chi-squared test revealed a significant relationship between BBB dysfunction incidence and time in the IPSI, but not CONTRA, hemisphere (C). * $P < 0.05$ ** $P < 0.01$ *** $P < 0.001$.

Figure 2-2. Representative images comparing X-ray fluorescence imaging of Gd (A) Fe (B), Cl (C) and K (D). The black line marks the hematoma boundary. Diffusion of ion dyshomeostasis and BBB permeability are more easily assessed using X-ray fluorescence imaging than cresyl violet staining (E). Cresyl violet staining confirms the hematoma boundaries determined with XFI. Tissue in the hematoma is more fragile and appears to have been damaged/destroyed in the staining process (E).

Figure 2-3. X-ray fluorescence analysis reveals that Ca, Cu, and Zn in the hematoma are unaffected by intracerebral hemorrhage at day 3 post-injury (A, C, H). Cl, Fe, Gd, and Mn concentrations in the IPSI hematoma were significantly increased as compared to CONTRA and SHAM hemispheres (B, D, E, G). K concentrations were significantly decreased in the IPSI hematoma as compared to CONTRA and SHAM hemispheres (F). * $P < 0.05$ ** $P < 0.01$ *** $P < 0.001$.

Figure 2-4. There was a distance main effect for Gd, Fe, and Cl, such that values were highest in the hematoma and decreased with distance into the perihematoma zone (A-C). There was a distance main effect for K, where values were lowest in the hematoma and normalized with distance into the perihematoma zone (D). * $P < 0.05$ as compared to CONTRA. † $P < 0.05$ as compared to SHAM. Hematoma is shown for reference but was excluded from the analyses.

Figure 2-5. The proportion of Cl and K variance accounted for by Gd concentration does not change with distance from the hematoma edge for most animals (A, C). Gd concentration can strongly predict Fe concentration close to the hematoma/PHZ interface. This effect disappears with distance into the PHZ (B). Each regression line represents a single sample. Red data points indicate a significant correlation.

LIST OF ABBREVIATIONS

| | |
|-----------|--|
| AWB | Autologous whole blood |
| BBB | Blood-brain barrier |
| BP | Blood pressure |
| CAA | Cerebral amyloid angiopathy |
| CNS | Central nervous system |
| EB | Evans blue |
| EC | Endothelial cell |
| GABA | γ -Aminobutyric acid |
| Hb | Hemoglobin |
| HO-1 | Heme oxygenase 1 |
| Hp | Haptoglobin |
| ICH | Intracerebral hemorrhage |
| ICP | Intracranial pressure |
| ICPMS | Inductively-coupled plasma mass spectrometry |
| ISC | Ischemic stroke |
| LAM | Leukocyte adhesion molecule |
| MMP | Matrix metalloproteinase |
| MM Φ | Microglia and macrophages |
| NVU | Neurovascular unit |
| PHZ | Perihematoma zone |
| SAH | Subarachnoid hemorrhage |
| SD | Standard deviation |
| TBI | Traumatic brain injury |
| tPA | Tissue plasminogen activator |
| VEGF | Vascular endothelial growth factor |
| XFI | X-ray fluorescence imaging |

CHAPTER 1

1.1 Introduction

This thesis describes changes in blood-brain barrier (BBB) permeability following intracerebral hemorrhage (ICH) and how it relates to early ion dyshomeostasis in a rodent model. An ICH occurs due to vessel rupture in the brain parenchyma and accounts for 10-15% of all strokes (Sacco et al., 2009). One form of secondary injury after ICH is BBB dysfunction, which causes edema and, presumably, functional deficits. We hypothesized that BBB damage would be highest at day 3 after ICH and would decrease thereafter. Furthermore, we hypothesized that BBB damage would be related to changes in chloride, potassium, iron, and other element levels in the brain at day 3 post-ICH. The underlying rationale will be explained in the following introductory sections. Background information on relevant topics, such as stroke epidemiology, experimental models of ICH, BBB injury, and acute ion dyshomeostasis is provided.

1.2 Stroke

1.2.1 Epidemiology

A stroke is a largely vascular event projected to cause 23 million deaths worldwide in 2030, making it the second leading cause of preventable death (World Health Organization, 2008, Kuklina et al., 2012). Approximately 16 million people suffer a stroke worldwide every

year (Mukherjee and Patil, 2011). Combined with heart disease, stroke is the leading cause of hospitalization in Canada (Heart and Stroke Foundation of Canada, 2015a). The Heart and Stroke Foundation of Canada recently estimated that over 62,000 Canadians have a stroke each year – that is, one stroke every nine minutes (Heart and Stroke Foundation of Canada, 2015b). ICH is a subtype of stroke characterized by the rupturing of blood vessels. While ICH accounts for only 10-15% of all strokes, it has a 40% 1-month mortality rate (Flaherty et al., 2010, Schlunk and Greenberg, 2015). Ischemic stroke (ISC) is the more common subtype of stroke and is characterized by impaired blood flow to the brain due to clot (Canadian Stroke Network, 2011).

In Canada, the estimated one-year economic burden of ISC alone is approximately \$2.8 billion including direct (*e.g.* hospitalization, rehabilitation, homecare) and indirect costs (*e.g.* unpaid caregivers, lost productivity) (Mittmann et al., 2012). When ICH is included, the economic burden increases to approximately \$3.6 billion (Canadian Stroke Network, 2011). Although stroke risk can be reduced (*e.g.* by minimizing stress and increasing physical activity), preventative interventions have only been moderately successful, even though such interventions could save the Canadian economy \$36.1 billion over 20 years (Canadian Stroke Network, 2011, Feigin et al., 2015). Low rates of stroke prevention success may be because many individuals are made aware of their stroke risk only after visiting a health care professional and, in general, only high-risk individuals are targeted by risk reduction campaigns (Feigin et al., 2015).

With advances in medical care, stroke mortality has declined to an average of 17%, and this has resulted in an increase in stroke survivors, of whom up to 75% are living with impairments (World Health Organization, 2008, Mukherjee and Patil, 2011, Heart and Stroke

Foundation of Canada, 2015b, Krueger et al., 2015, Sacco et al., 2016). Stroke mortality is 25% higher in low- and middle-income countries than in high-income countries (Mukherjee and Patil, 2011). Meta-analysis suggests that ICH mortality has not changed in the past few decades, although one recent population-based study suggests that 1-year ICH mortality rates have decreased by 19% in the past two decades (van Asch et al., 2010, Sacco et al., 2016). Despite many clinical trials for various post-stroke pharmacological interventions, only one agent, tissue plasminogen activator (tPA), a clot-busting drug, has shown success and is in clinical use. Only ~10% of stroke patients are eligible to receive tPA, however, because it is predominantly used to treat ISC, has a narrow therapeutic window, and can cause deleterious side effects (Jauch et al., 2013). Acutely, ICH patients may be treated with hemostatic agents to minimize bleeding, with drugs to manage blood pressure, or, in patients with rapid deterioration, with surgery to evacuate the hematoma (Morotti and Goldstein, 2016). It should be noted that there are no gold-standard treatments, with the aforementioned treatments based on clinical trials (*e.g.* the FAST, ATACH, and STICH trials) with inconclusive results (Gonzales, 2013). Thus, these therapies have no proven efficacy as of yet. Physical rehabilitation is commonly used to reduce disabilities after ICH (Liu et al., 2014, Nadeau et al., 2015, Saulle and Schambra, 2016), although optimal parameters for treatment have not yet been fully elucidated (Saulle and Schambra, 2016). One potential obstacle is that, compared to ISC, relatively little research has been done to understand the mechanisms underlying and the optimal parameters for rehabilitation after ICH.

1.2.2 Intracerebral Hemorrhage

Hemorrhagic stroke occurs when blood vessels rupture in the parenchyma or the subarachnoid space (subarachnoid space; SAH). SAH are relatively rare, accounting for roughly 5% of stroke cases, and are commonly caused by traumatic brain injury (TBI) or ruptured aneurysms (Abraham and Chang, 2016). ICH accounts for 10-15% of all stroke cases, but accounts for over 20% of cases in patients under 45 (Sacco et al., 2004). Mortality rates are as high as 35%, 48% and 57% for 7 day, 30 day, and 1 year survivals, respectively (Marini et al., 2001, Sacco et al., 2009). Those with diabetes have higher mortality rates at days 7 and 30, and elderly patients had higher mortality at day 30 in a prospective population-based study (Sacco et al., 2009). SAH victims have similar mortality rates as compared to ICH (Hop et al., 1997). Despite these high mortality rates, it has been suggested that ICH *survivors*, as compared to ISC, have better short- and long-term outlooks (Kelly et al., 2003, Katrak et al., 2009, Hemphill et al., 2015). One proposed mechanism underlying this finding is that edema is resolved faster in perihematoma tissue than peri-infarct tissue, although this needs to be further studied (Kelly et al., 2003).

Clinically, the majority of hemorrhaging occurs at the ictus, with larger hemorrhages negatively correlated with functional outcome (Fieschi et al., 1988, Flaherty et al., 2010, Dowlatshahi et al., 2011b). In approximately 30% of patients, hematoma expansion occurs in the first day (Xi et al., 2006). Furthermore, an estimated 10-40% of ISC victims have hemorrhagic transformation (Fiorelli et al., 1999, Balami et al., 2011, Jickling et al., 2014).

There has been a recent rise in ICH due to increases in anticoagulant prescription and the use of tPA to reduce ISC severity/injury (Flaherty et al., 2010, Jickling et al., 2014). Anticoagulant use is now responsible for ~20% of ICH cases in the United States (Flaherty et al., 2010). These anticoagulants, such as warfarin and novel oral anticoagulants, may transform asymptomatic microhemorrhages, of which there are an estimated 2 million per year in the USA, into a symptomatic ICH (Leary and Saver, 2003). Indeed, warfarin use increases risk of microbleed transformation into symptomatic ICH (*i.e.* associated with neurological changes and/or death) 80-fold (Lee et al., 2009).

1.2.2.1 Clinical Manifestation

An ICH occurs most frequently in the basal ganglia (~40%), followed by the cortex (~25%), the thalamus (~15%), the cerebellum (~10%), and the pons (~5%) (Sacco et al., 2004). Intraventricular hemorrhage is associated with mortality rates of 60-90% (Broderick et al., 2007). Neurological consequences such as nausea and vomiting (29-46% of patients), severe headache (33-57%), increased blood pressure (BP; ~70%) and decreased consciousness (28-37%) are common following ICH (Balami and Buchan, 2012, Ko et al., 2012, Hemphill et al., 2015). Seizures occur in 4 - 28% of patients (Qureshi et al., 2009). Approximately 8% of ICH patients have seizures at ICH onset, while ~8% and 3% of patients have seizures early (*i.e.* within 2 weeks of ICH) and late (*i.e.* later than 2 weeks after ICH), respectively (Bogousslavsky et al., 1988, Bladin et al., 2000). Late, but not early, seizures are associated with poor outcome and high mortality (De Herdt et al., 2011, Rossi et al., 2013, Li et al., 2015). Importantly, it is difficult to accurately estimate seizure incidence without the use of continuous EEG monitoring,

as many seizures may be subclinical (*i.e.* not presenting with clinical signs or symptoms) (Balami and Buchan, 2012).

Hemorrhage size and location are important predictors of outcome (Broderick et al., 1993, Xi et al., 2006). Hematomas greater than 2 cm in diameter or 10 cm³ cause increased intracranial pressure (ICP), whereas those larger than 4 cm in diameter are generally fatal (Sacco et al., 2004, Ko et al., 2012). Importantly, while elevated ICP may predict outcome at 30 days post-ictus, it is the variability (*i.e.* magnitude and duration of pressure fluctuations) in ICP that best predicts outcome (Tian et al., 2013).

Cerebellar and medullar ICH victims often present with coma and have a poor outlook (Sacco et al., 2004). In addition, larger or more severe ICH tends to present with decreased consciousness, possibly due to elevated ICP (Sacco et al., 2004). Those with lobar hemorrhages, as compared to deep and infratentorial, are more likely to have better functional outcomes and quality of life (Sreekrishnan et al., 2016). A recent meta-analysis suggests that hemorrhage hemisphere is not a good predictor of outcome, although future studies assessing this should include both motor- and cognition-based endpoints (Sreekrishnan et al., 2016).

1.2.2.2 Risk Factors

The biggest risk factors for ICH are age, hypertension (*i.e.* high BP), cerebral amyloid angiopathy (CAA), and other vascular factors (Flaherty et al., 2010, Schlunk and Greenberg, 2015). Hypertension accounts for up to two-thirds of ICH (Keep et al., 2014). Chronic hypertension induces cerebrovascular remodeling. Reactive oxygen species production is upregulated in vessel walls, resulting in increased cell proliferation, increased vessel stiffness,

altered cytoskeletal organization, and smooth muscle cell rearrangement, among others (Montezano et al., 2015). Chronic hypertension also causes microaneurysms in arterioles and small vessel damage (Fisher, 1971, 1972).

CAA, resulting from β -amyloid deposition in cerebral small vessels, causes vessel damage and, subsequently, microbleeds and lobar ICH (Viswanathan and Greenberg, 2011, Samarasekera et al., 2012). CAA accounts one-third of ICH in elderly populations (Sacco et al., 2004). Furthermore, as CAA is a hallmark of Alzheimer's disease pathology, patients with Alzheimer's disease have a high risk of ICH (Viswanathan and Greenberg, 2011).

Race and sex are non-modifiable risk factors for ICH. The Longitudinal Reasons for Geographic and Racial Differences in Stroke (REGARDS) study found a race by age interaction. Those of African descent had no change in risk between ages 45 and 85, but were 5 times as likely than white patients to have a stroke at 45. Risk of stroke doubled every decade after 45 years old in white patients. In agreement with other studies, males of both races had higher ICH risk than females (Howard et al., 2013). ICH risk is higher for Asian populations than all other ethnicities, although 1-month mortality rates tend to be lower (Adeoye and Broderick, 2010, van Asch et al., 2010). Sex differences in ICH incidence in Asians are likely mediated by alcohol consumption (van Asch et al., 2010).

Many risk factors for ICH are modifiable and include alcohol consumption, diabetes (to an extent), diet, and exercise. These factors increase risk because they contribute to poor cardiovascular health (Poon et al., 2015).

1.2.3 Rodent models of intracerebral hemorrhage

The two most widely used animal models of ICH are the autologous blood injection and the collagenase injection models. Each model has different characteristics relevant to ICH. The autologous whole blood (AWB) model relies on infusing a clinically relevant volume of blood into the parenchyma and results in blood accumulation (modeling the hematoma), reduced cerebral blood flow, and edema. Injections of collagenase, on the other hand, disintegrate the basal lamina of blood vessels, leading to spontaneous bleeding, hematoma expansion, and edema (Yan et al., 2015). In comparison to the AWB model, the collagenase model results in ongoing bleeding, greater and increasing BBB injury, more severe and more persistent functional deficits, greater tissue loss, greater edema, greater inflammation, and more extensive white matter damage (Table 1-1) (Xue and Del Bigio, 2003, MacLellan et al., 2008, Kirkman et al., 2011, Manaenko et al., 2011).

Because ICH is induced in different ways between the two models, it is expected that different damage and plasticity pathways are activated. Indeed, various therapies have been tested in both models of ICH, with inconsistent or conflicting results found across models. For example, although rehabilitation consistently improves functional recovery following ICH, changes in lesion volume, dendritic complexity, and mechanisms vary by model (MacLellan et al., 2011, Caliaperumal and Colbourne, 2014). These differences hold true for hypothermia as well. In the AWB model, two days of mild therapeutic hypothermia induced at 1 or 4 hours post-ICH was found to reduce edema, BBB disruption, and inflammation without aggravating bleeding or attenuating functional deficits (MacLellan et al., 2006b). However, hypothermia given within 12 hours after collagenase injection was found to increase hematoma volume as compared to normothermic controls (John et al., 2015, Wowk et al., 2016).

Due to the differences in pathophysiology between models, they vary in clinical relevance and may impact translational value (Table 1-1). Failure to translate is a major concern in stroke research. For example, of 1,026 treatments tested in ISC, only tPA was successful (O'Collins et al., 2006). In ICH, many issues may contribute to translational failures, such as flawed experimental design, poor data analysis, and over-reliance on certain endpoints (MacLellan et al., 2012). Furthermore, the majority of research has examined ICH in young, male rats. As ICH impacts both sexes and is more common in older individuals, translational value of the aforementioned research is limited (Kirkman et al., 2011). Rodents are the most commonly used animals in preclinical stroke research. However, due to their relative dearth of white matter in comparison to humans, rodent models do not always translate well for certain endpoints (*e.g.* edema) (Wagner and Zuccarello, 2009, Venkatasubramanian et al., 2011). As ICH is a heterogeneous condition (*i.e.* due to various and/or multiple causes; with various forms of injury), it is understandable that there is no perfect preclinical model. Therefore, for greatest translational value, researchers should test neuroprotective therapies (*e.g.* pharmacological interventions and rehabilitation) in multiple models and multiple settings.

1.2.4 Pathophysiology of intracerebral hemorrhage

ICH causes two general types of damage. Primary, mechanical damage occurs when blood from the initial rupture dissects through surrounding tissue (Schlunk and Greenberg, 2015). This is compounded by ischemic injury in the center of the hematoma, where the ruptured and damaged vessels can no longer supply adequate blood to region (Knight et al.,

2008). Secondary damage occurs in the perihematoma zone (PHZ), which is the region of tissue immediately surrounding the hematoma. Secondary damage is characterized by cell death, oxidative damage, and inflammation. Although the complete set of secondary events and their contributions to tissue damage and functional deficits have not been fully elucidated, the activation of multiple pathways by intraparenchymal blood most likely mediates the majority of damage (Aronowski and Zhao, 2011, Schlunk and Greenberg, 2015). Primary damage will be described. The resulting cytotoxicity of blood and plasma components will then be discussed. Other forms of secondary injury (*e.g.* edema, inflammation) will be later discussed in relation to BBB dysfunction.

1.2.4.1 Primary damage

Primary damage after ICH is predominantly mechanical and is associated with mass effect (*i.e.* the displacement of surrounding tissue) (Qureshi et al., 2009, Aronowski and Zhao, 2011). This mechanical damage results from blood tearing through the parenchyma. This causes disruption of vessels, neurons, their axons, and glia as well as neurotransmitter release, mitochondrial dysfunction, and membrane depolarization. Ultimately, this damage is associated with metabolic dysregulation and cell death (Qureshi et al., 2009). Primary damage also occurs during hematoma expansion. In most patients, bleeding stops within 3 hours; however, delayed hematoma expansion may occur days to weeks later (Xi et al., 2006, Dowlatshahi et al., 2011a, Delcourt et al., 2012). Despite ischemic injury in the hematoma, multiple experimental and clinical studies have shown that reductions in peri-hematoma blood flow due to mass effect and hematoma expansion are not sufficient to induce ischemia (Zazulia et al., 2001, Herweh et al., 2010, Kate et al., 2014).

1.2.4.2 Secondary damage

Secondary damage resulting from the release of blood into the parenchyma follows primary damage and impacts initially healthy PHZ tissue.

1.2.4.2.1 Thrombin

Thrombin contributes to blood clotting and is rapidly produced in response to the initial hemorrhage (*e.g.* within 3 hours in animal models) (Wu et al., 2010). Initial production of thrombin is protective, as it leads to blood clotting and may prevent hematoma enlargement. However, higher concentrations of thrombin contribute to inflammation, edema, cell death, and increased blood-brain barrier infiltration, at least in animal models (Hua et al., 2007).

Simplified models of ICH involve injection of components known to contribute to secondary damage. Thrombin injection into the parenchyma alone causes BBB damage by disrupting the endothelium (Lee et al., 1997, Liu et al., 2010). This damage may be partially mediated by protease activated receptors, as inhibition of these receptors attenuates BBB damage in an intraventricular hemorrhage model (Gao et al., 2014). Thrombin may also indirectly impact BBB function, as thrombin injections induce a large inflammatory response (Masada et al., 2001, Moller et al., 2006). Furthermore, even using an injection volume comparable to the amount of thrombin produced in mild ICH, thrombin causes dendritic atrophy and cell death without contributing to the chronic tissue loss seen in ICH (Caliaperumal et al., 2014).

Many therapies aim to modulate thrombin-mediated injury, with delayed therapies aiming to reduce thrombin production. Thrombin inhibitors, such as argatroban, have been

shown to reduce edema formation when administered at least 3 hours post-ICH in the AWB model (Kitaoka et al., 2002). Conversely, therapies are given acutely aim to promote thrombin production to limit hematoma volume. Recombinant Factor VIIa, a hemostatic agent that promotes coagulation by increasing thrombin production, has been shown in preclinical and clinical studies to reduce hematoma volume (Kawai et al., 2006, Mayer et al., 2008, Nadeau et al., unpublished). Interestingly, at least clinically, such improvements may not impact functional outcomes, and use of the drug can lead to thromboembolic events (Mayer et al., 2008). Other early treatments may worsen thrombin-mediated injury. For example, hypothermia worsened neuronal degeneration in the thrombin injection model when given shortly after ICH (Wowk et al., 2014).

1.2.4.2.2 Hematoma resolution and blood cytotoxicity

Once blood is released into the parenchyma following the initial rupture, the fate of erythrocytes and their by-products varies. Hematoma resolution, or the removal of blood from affected tissue, is generally thought to begin with erythrocyte lysis, which starts approximately one day after ICH and leads to hemoglobin (Hb) release (Wagner et al., 2003, Dang et al., 2017). Hb can then spontaneously oxidize, producing ferric heme and superoxide (Chen-Roetling et al., 2015). In turn, the superoxide dismutase generates hydrogen peroxide (Alayash, 2006). All three products can cause oxidative damage to lipids, proteins, and DNA in the PHZ (Stankiewicz et al., 2007). Heme and hemin (oxidized heme) can bind to hemopexin, and these complexes are endocytosed by CD91-expressing macrophages. Because hemopexin exists in relatively low quantities in the brain and is easily depleted, neurons and astrocytes uptake toxic quantities of hemin after ICH. As a result, some hemin is transported extracellularly via ferroportin (an iron

efflux channel) and contributes to oxidative stress and tissue damage (Chen-Roetling et al., 2015).

Heme oxygenase-1 (HO-1) is the rate-limiting enzyme for the breakdown of the hemoglobin into its constituent parts: iron, carbon monoxide, and biliverdin (Abraham and Kappas, 2008). HO-1 is upregulated in the presence of heme, among other factors, causing the normally low levels of HO-1 to increase, peaking at day 3 post-ICH and persisting to at least day 28 (Wu et al., 2003, Chen-Roetling et al., 2015). As bilirubin, a metabolite of biliverdin, is an antioxidant, HO-1 activity protects against oxidative damage in the early stages following ICH (Abraham and Kappas, 2008, Jansen et al., 2010, Wang et al., 2011). However, this elevation in HO-1 lasts to at least day 14, leading to free iron accumulation and oxidative damage (Wang et al., 2011).

In sum, Hb by-products and HO-1 contribute to tissue damage in the PHZ. Notably, the sole injection of blood components, such as lysed erythrocytes, hemoglobin, and iron, all induce BBB dysfunction leading to edema, cell death and behavioral dysfunction (Xi et al., 2001, Katsu et al., 2010, Zhao et al., 2011, Yang et al., 2013).

Endogenous mechanisms exist to prevent blood cytotoxicity. For example, Hb may bind to haptoglobin (Hp), a protein produced by hepatocytes and oligodendrocytes. Following erythrocyte lysis, the Hp-CD163-heme oxygenase-1 pathway immediately acts to remove free circulating Hb. Hb readily binds to Hp, creating a complex that is easily taken up by macrophages via the CD163 receptor (Thomsen et al., 2013). CD163 is expressed on macrophages, astrocytes, and neurons following ICH and is affected by a variety of factors (*e.g.*

pro- and anti-inflammatory factors) (Dang et al., 2017). Notably, CD163 can take up free hemoglobin when Hp levels are depleted, provided all receptors are not saturated. Hp defenses are easily overwhelmed acutely, and Hp levels are not restored until 5 to 7 days post-ICH (Aronowski and Zhao, 2011). In response to increased CD163 expression, HO-1 and IL-10 upregulation are seen. Furthermore, ferritin (an iron storage protein) is upregulated in response to HO-1 upregulation (Regan et al., 2002). In this way, activation of the Hp-CD163-heme oxygenase-1 pathway has anti-oxidant and anti-inflammatory effects.

1.3 Blood-brain barrier dysfunction following intracerebral hemorrhage

Injury to the BBB is a hallmark of many CNS pathologies including ICH (Abbott et al., 2010). Here, intact BBB physiology will be described. BBB dysfunction and its relation to other forms of secondary injury following ICH will then be discussed.

1.3.1 Blood-brain barrier physiology

1.3.1.1 Function

The BBB acts as an interface between circulating blood and the central nervous system (CNS) and facilitates proper brain function by maintaining homeostasis (Siegenthaler et al., 2013, Andreone et al., 2015). The BBB has many functions. It maintains ion levels (*e.g.* Na⁺, Cl⁻, K⁺), controls neurotransmitter entry into the CNS, prevents macromolecule and neurotoxin entry into the CNS (thereby preventing the associated apoptosis and tissue damage), and

ensures adequate nutrient supply (Abbott et al., 2010). BBB structure is optimized for these functions.

1.3.1.2 Structure

The neurovascular unit (NVU) is a multicellular system composed of endothelial cells (EC), neurons, pericytes, and glial cells that comprises the blood-brain barrier (BBB) to control the efflux and influx of substances for proper neurotransmission and limit passive diffusion of compounds between the blood and the brain (Figure 1-1) (Siegenthaler et al., 2013, Andreone et al., 2015). Only lipophilic and very small molecules (< 400 Da) may freely pass through the BBB.

In general, ECs are crucial for maintaining BBB integrity (Andreone et al., 2015). ECs are linked by tight junctions, which prevent passage of water-soluble molecules, macromolecules, ions, and nutrients in the paracellular space and into the CNS (Hawkins and Davis, 2005, Abbott et al., 2010). ECs of the BBB also have lower rates of transcytosis than peripheral ECs and are therefore less leaky. In the CNS, ECs instead rely upon a diverse array of transporters (*e.g.* glucose transporter, Glut1; efflux transporter, P-glycoprotein) to selectively deliver nutrients and ions and remove harmful substances (Siegenthaler et al., 2013). However, transcytosis remains the main mechanism for macromolecule entry into the parenchyma (Abbott et al., 2010). Finally, the ECs of the BBB prevent entry of immune cells into the CNS due to their relatively low expression of leukocyte adhesion molecules (LAMs), which control the entry of inflammatory cells into the CNS (Rossler et al., 1992).

Astrocyte support feet interface with the basal lamina of ECs (Abbott et al., 2006).

Astrocytes help facilitate BBB function. They regulate tight junction component expression and integrity by secreting Sonic hedgehog and angiotensinogen/angiopoietin-1, respectively (Lee et al., 2003, Wosik et al., 2007, Alvarez et al., 2011). Pericytes, which attach to both ECs and astrocytes, play a key role in modulating BBB leakiness and CNS immune cell entry. For example, in pericyte-deficient experimental models, pericyte loss is associated with increased vascular permeability, higher levels of transcytosis, and increased LAM expression and subsequent immune cell entry (Armulik et al., 2010, Daneman et al., 2010).

The NVU supports neurovascular coupling. Astrocytes and pericytes contribute to neurovascular coupling, a functional matching between neurons and blood vessels whereby demands for glucose and oxygen are communicated (Bell et al., 2010, Petzold and Murthy, 2011). Accordingly, cerebral blood flow increases in areas with active neurons.

1.3.2 Blood-brain barrier permeability in intracerebral hemorrhage patients

After ICH, BBB dysfunction is biphasic. Acute BBB dysfunction occurs during the initial vascular disruption of the hemorrhage, and later dysfunction is indicative of secondary injury (*e.g.* inflammation) or repair (*e.g.* angiogenesis) processes. Indeed, contrast agent extravasation (indicative of increased BBB permeability) has been noted in early (*i.e.* within 24 hours) and late (*i.e.* one week) after ICH (Murai et al., 1998, Hallevi et al., 2010). In a small prospective study with BBB damage measured approximately 8 days post-ICH, there was high permeability in perihematoma tissue and low to no BBB damage in the contralesional hemisphere (Aksoy et al.,

2013). Patients with large ICH had greater and more variable BBB damage than patients with small hemorrhages. Lobar hemorrhages tended to have greater BBB permeability than deep ICH, perhaps due to differences in vascular patterns between regions and differences in etiology. For example, CAA is often an underlying cause of lobar hemorrhage, whereas hypertension is a greater risk factor for subcortical hemorrhage(Charidimou et al., 2012). BBB damage is significantly lower in hypertension-associated ICH than in ICH due to other causes. BBB damage predicts early (day 1) but not late edema (day 7) (Aksoy et al., 2013). Others estimate that 75% of patients have BBB damage in the PHZ 5 days after ICH (Kidwell et al., 2011).

1.3.3 Monitoring blood-brain barrier permeability

BBB permeability is assessed in patients and in animal models using either endogenous or exogenous tracers. These tracers would not be able to enter a brain with an intact BBB. Extravasated blood proteins may be detected in the parenchyma by using antibodies conjugated to horseradish peroxidase (Schmidt-Kastner et al., 1993). This method, although it avoids the confounds of injecting a foreign compound, is not sensitive enough to detect extravasation of small molecules and only measures total extravasation since injury. Use of exogenous tracers is generally preferred due to the variety of molecular weights available. In animal models, Evans blue (EB) dye is commonly used. EB binds to the macromolecule albumin and can be quantified in tissue sections visually or using spectrophotometry (Radu and Chernoff, 2013). Use of EB may lead to an overestimation of BBB damage due to its reversible

binding kinetics with albumin. Dextran-based dyes are available in a variety of molecular weights to directly assess BBB permeability to different sized molecules (Kassner and Merali, 2015). Importantly, the BBB may open to large molecules while still restricting movement of small ions and vice versa, so BBB permeability data should be carefully interpreted (Kang et al., 2013).

In humans, magnetic resonance imaging of gadolinium-based contrast agents has been used to assess BBB permeability in a wide range of CNS disorders for over 25 years. This method allows spatial assessment of BBB injury in both white and gray matter with few to no side effects (Montagne et al., 2016). This technique may be successfully used to predict hemorrhagic transformation following thrombolytic therapy in ISC (Scalzo et al., 2013). Increased BBB permeability precedes hemorrhage, and the magnitude of gadolinium extravasation prior to thrombolytic therapy administration is strongly correlated with hematoma volume in patients with hemorrhagic transformation (Kastrup et al., 2008, Leigh et al., 2014).

1.3.4 Pathophysiology

Edema and leukocyte extravasation are consequences of BBB dysfunction after ICH (Keep et al., 2014). BBB dysfunction post-ICH is characterized by increased permeability due to paracellular alterations and transcellular changes and results from direct and indirect damage to the BBB (Knowland et al., 2014). For example, as previously mentioned, many blood

components induce BBB dysfunction (Xi et al., 2001, Katsu et al., 2010, Zhao et al., 2011, Yang et al., 2013).

In the AWB model of ICH, there is delayed BBB disruption, with no measurable damage at 4 hours or 8 hours but progressively increasing damage from 12 to 48 hours or at 24 hours in rats and pigs, respectively (Yang et al., 1994, Wagner et al., 1996, Wagner et al., 1999, Adeoye and Broderick, 2010). In the collagenase model, BBB permeability is increased from 5 hours to 7 days post-injection, and BBB permeability did not significantly differ from control samples at day 14 (Rosenberg et al., 1993). High BBB permeability has been detected in the hematoma, but not PHZ, 12 hours post-collagenase injection, with BBB hyperpermeability increasing to at least day 4 in the hematoma and PHZ (MacLellan et al., 2008). Importantly, it is unclear whether the prolonged BBB damage results from lasting collagenase-induced basal lamina degradation or from hematoma resolution processes (Keep, 2008). The collagenase model, despite its limitations, best mimics clinical BBB damage following ICH due to the temporal profile of BBB permeability. The AWB model, with low constant levels of BBB permeability, does not seem mimic clinical data as well.

1.3.4.1 Inflammation

Inflammatory response begins almost immediately following ICH and mediates secondary damage (Chen et al., 2015). As previously mentioned, thrombin indirectly and directly contributes to the inflammatory response and BBB dysfunction (Lee et al., 1997, Masada et al., 2001, Moller et al., 2006, Liu et al., 2010). In animal models, neutrophils may infiltrate the PHZ within 4 hours of ictus, and levels peak between 2 to 3 days later (Gong et al.,

2000, Xue and Del Bigio, 2000, Wang and Dore, 2007). As the source of matrix metalloproteinases (MMPs; enzymes that degrade extracellular matrix proteins) and TNF α (inflammatory modulators), early neutrophil infiltration influences further leukocyte response (Wasserman and Schlichter, 2007, Moxon-Emre and Schlichter, 2011). Microglia and macrophages (MM Φ) are the primary agents responsible for hematoma clearance, along with circulating inflammatory cells. Microglia levels increase in response to the presence of hematoma degradation products (*e.g.* hemoglobin), however, and activate numerous inflammatory response pathways that contribute to brain injury. Therefore, inhibiting microglia activation can attenuate some forms of damage, such as edema and BBB leakage (Yan et al., 2015). The inflammatory response leads to the release of cytokines such as TNF α (Zhou et al., 2014). TNF- α is upregulated in the presence of thrombin and may contribute to edema, as TNF- α knockout mice have reduced edema following experimental ICH as compared to wild-type mice (Hua et al., 2006). Interestingly, BBB dysfunction precedes inflammatory response in ISC and facilitates the entry of immune cells into the parenchyma (Schoknecht et al., 2015). Inflammation itself may induce BBB permeability through the release of MMPs (Gidday et al., 2005).

1.3.4.1.1 Vascular integrity

MMPs are generated by the immune response and act by degrading extracellular matrices. MMP-9 degrades the basal lamina of vessels and is upregulated following ICH in animal models and patients (Florczak-Rzepka et al., 2012, Hartz et al., 2012). This weakens vessels, making them more vulnerable to rupture and subsequent micro-hemorrhaging (Gasche et al., 1999, Gidday et al., 2005). Predictive markers of hemorrhagic transformation in ISC are

BBB dysfunction and elevated MMP-9 levels (Montaner et al., 2001, Montaner et al., 2003, Castellanos et al., 2007). In a case study assessing MMP expression in infarcted and hemorrhagic tissue following hemorrhagic transformation, elevated MMP-9 levels were found in hemorrhagic tissue and were associated with basal lamina degradation and BBB dysfunction (Rosell et al., 2008). Furthermore, MMPs contribute to BBB dysfunction by degrading tight junctions (Yang et al., 2007, Sandoval and Witt, 2008, Lischper et al., 2010, Yang and Rosenberg, 2011, Liu et al., 2012). In a stroke-prone spontaneously hypertensive model of ICH, BBB dysfunction preceded ICH, further supporting the idea that weakened vessels are more vulnerable to rupture (Lee et al., 2007). MMP-9 independently predicts outcome but not edema after ICH (Li et al., 2013). MMP inhibitors, such as the MMP-2 inhibitor TIMP2, have been shown to attenuate BBB dysfunction in experimental ICH (Rosenberg et al., 1992).

1.3.4.2 Edema

Edema, the accumulation of water in brain tissue, occurs after ICH as a result of a variety of factors such as BBB dysfunction, mass effect, and the activation of inflammatory pathways by thrombin. Serum extrusion into the parenchyma occurs hyperacutely. Acute ionic edema is attributed to extravasation of electrolytes and water from damaged blood vessels/disrupted BBB integrity (Lim-Hing and Rincon, 2017). Clinically, peak edema is seen at 12 days post-ICH, and edema growth in the first two days following ICH is negatively correlated with functional outcome (Venkatasubramanian et al., 2011). Delayed edema, occurring several days post-ICH, is most likely attributable to hematoma resolution (Wu et al., 2006). Macromolecule extravasation (*e.g.* albumin) following BBB injury contributes to vasogenic edema, whereas cell death contributes to cytotoxic edema (Schoknecht et al., 2015, Lim-Hing and Rincon, 2017).

The Intensive Blood Pressure Reduction in Acute Cerebral Hemorrhage Trial

(INTERACT)¹ and INTERACT² clinical trials examined the relationship between edema and functional outcome, as well as the therapeutic efficacy of an intensive blood pressure lowering regimen (Yang et al., 2015). Not only did perihematomal edema growth predict hematoma volume and growth, it also independently predicts outcome, especially in patients not receiving the intensive regimen. This implies that early intervention with a blood pressure reduction regimen following ICH is safe and may limit perihematomal edema growth (Gould et al., 2014, Yang et al., 2015). Despite these findings, some have found that edema does not predict functional outcome when hematoma size is controlled (Appelboom et al., 2013). Others still find that edema only predicts outcome for certain stroke subtypes (*e.g.* mild basal ganglia stroke) (Murthy et al., 2015). In patients enrolled in the ICH ADAPT trial receiving BP reduction treatment, BBB permeability was elevated in the hematoma and PHZ in the first 24 hours after stroke. Interestingly, BBB permeability was unrelated to hematoma volume, edema, edema growth, or BP reduction in both treatment groups (McCourt et al., 2015). In sum, BBB dysfunction may contribute to different forms of edema in both experimental and clinical populations.

1.3.4.3 Angiogenesis

Unfortunately, there is limited data available regarding angiogenesis after ICH. Vascular endothelial growth factor (VEGF) mediates vascular development by binding to fms-related tyrosine kinase 1 (Flt-1) and kinase insert domain (Flk-1) receptors in ECs and can rapidly induce BBB permeability (Dvorak et al., 1995, Veikkola and Alitalo, 1999). Angiopoietins, specifically Ang 1, are also involved in vascular remodeling and counterbalance VEGF activity by limiting

BBB permeability in mature, developed vasculature (Thurston et al., 1999). In a study assessing the relationship between BBB damage and angiogenesis in experimental ISC, Zhang and colleagues found that VEGF and Ang 1 mediated acute BBB dysfunction in the core and regulated late vascular remodeling in the penumbra. Unsurprisingly, as both are mediated by Ang 1 and VEGF, angiogenesis and BBB leakage were spatially and temporally related (Zhang et al., 2002). Elevated VEGF levels persisted to day 28 in that model. As VEGF is persistently elevated in injured tissue in ICH, angiogenesis may also induce late BBB leakage after ICH (Lei et al., 2015). Indeed, late vasogenic edema has been noted in neuroimaging studies and may reflect angiogenesis (Zazulia et al., 1999).

Changes in vessel density indicate angiogenesis. In animal models, increased vessel density and VEGF levels are observed between days 7 and 14 post-ICH using Western blotting and immunohistochemistry (Lei et al., 2015). Clinically, in ISC, angiogenesis may facilitate functional recovery in some populations while having deleterious effects in others (Krupinski et al., 1994, Szpak et al., 1999). In the collagenase model of ICH, VEGF, Flt-1, and Flk-1 are elevated in the PHZ beginning 2 days and persisting to at least 28 days post-ICH. Furthermore, new ECs (*i.e.* those labelled with BrdU and vWF) in microvessels can be detected in the PHZ from 2 to 14 days after injury (Tang et al., 2007).

Angiogenesis likely contributes to late BBB permeability. Delayed changes in the NVU, including the BBB, indicate a shift from injury to repair as it facilitates angiogenesis and other processes (Arai et al., 2009).

1.3.4.4 Ion dyshomeostasis

As previously mentioned, neurovascular coupling ensures adequate blood supply to active neurons. A strong neurovascular response (*e.g.* in seizure activity, ISC) and the associated increase in cerebral blood flow can therefore contribute to local ion dyshomeostasis with increases in extracellular potassium (Meldrum and Nilsson, 1976). Changes in ion transport channels may result in ion dyshomeostasis and edema. Indeed, changes in NKCC1, a Na-K-Cl cotransporter, mediate astrocytic swelling and edema after ischemic injury (Chen and Sun, 2005). Changes in extracellular potassium may also result from alterations in network excitability and are mediated by astrocyte activation and BBB dysfunction (David et al., 2009).

Ion dyshomeostasis can be assessed using X-ray fluorescence imaging (XFI). In this method, tissue samples are exposed to high energy x-rays, after which the sample will emit characteristic energy spectra that are detected with a specialized detector. Elemental concentrations can then be determined based on emitted wavelengths. XFI has been used in ICH previously (Hackett et al., 2015, Williamson et al., 2017). Other methods used to assess ion dyshomeostasis include inductively-coupled plasma mass spectrometry (ICPMS) and electron probe microanalysis.

Here, post-ICH ion dyshomeostasis will be discussed as a form of secondary injury and in relation to BBB injury.

1.3.4.4.1 Iron dyshomeostasis

Iron is essential for many biological processes, including oxygen transport and neurotransmitter production. However, iron accumulation contributes to motor and cognitive dysfunction, oxidative damage, and cell death (Stankiewicz et al., 2007). These detriments are

compounded by iron released in ICH. Under normal physiological conditions, any free iron is rapidly bound to transferrin, an iron carrier, and transported intracellularly (Wu et al., 2003, Stankiewicz et al., 2007). Ferritin then binds intracellular iron, with heavy chain ferritin associated with iron utilization and light chain associated with iron storage (Stankiewicz et al., 2007). Following ICH, levels of ferritin and transferrin are elevated. In the AWB model, both ferritin and transferrin levels were significantly elevated as compared to normal tissue on day 3. Peak levels occurred at day 7, with elevations persisting to at least day 28 (Wu et al., 2003). A similar pattern occurs in the collagenase model (Wang et al., 2016). High levels of transferrin increase intracellular free iron, leading to cytotoxicity. Therefore, high levels of ferritin are generally protective. However, it should be noted that iron can be toxic even when bound to ferritin (Siesjo et al., 1989). To investigate iron toxicity, researchers inject FeCl_2 into the parenchyma. One hallmark of this model is DNA damage, suggesting that iron contributes largely to oxidative stress following ICH (Nakamura et al., 2006). This model results in behavioral deficits, tissue loss, and neuronal degeneration (Caliaperumal et al., 2013). Iron accumulation following ICH due to the saturation of iron homeostatic mechanisms contributes to DNA and protein oxidative damage, with peak damage at day 3 in the FeCl_2 model of ICH (Nakamura et al., 2006). Indeed, saturation of transferrin results in significant increases in interstitial free iron (Wagner et al., 2003). Fe^{2+} reacts with hydrogen peroxide, generating Fe^{3+} , HO^- , and $\text{HO}\bullet$, and causing oxidative stress and neuronal damage (Figure 1-2) (Prousek, 2007). Of note, others argue iron toxicity may not be the primary mediator of secondary damage (Zille et al., 2017). Regardless, increased iron in the brain contributes to increased BBB permeability (Zhao et al., 2011).

1.3.4.4.1.1 Oxidative stress

Oxidative stress following ICH causes extensive tissue damage and results from free radical accumulation, iron dyshomeostasis, and depletion of endogenous antioxidant mechanisms. Much support for oxidative stress as the main factor mediating secondary damage comes from studies showing the efficacy of free radical scavengers such as deferoxamine and NXY-059. Administration of these agents reduce injury in experimental ICH, although this effect is not consistent across studies (Warkentin et al., 2010, Aronowski and Zhao, 2011). Both deferoxamine and NXY-059 have been tested in clinical trials. While NXY-059 had no adverse side effects, it had no effect on functional outcome 3 months after ICH (Lyden et al., 2007). Phase II trials for deferoxamine are currently underway (Yeatts et al., 2013).

Impaired antioxidant defense systems contribute to oxidative stress after ICH (Hu et al., 2016). The Keap1-Nrf2 pathway is a major endogenous antioxidant pathway. In the AWB model, this pathway is upregulated within 24 hours of insult (Shang et al., 2013). Nrf2 mediates antioxidant homeostasis and is activated by the compound sulforaphane. Administration of sulphoraphane after ICH upregulates antioxidant activity, reduces tissue damage, and attenuates functional deficits, although this, once again, has failed to replicate across all models and environments (Zhao et al., 2007, Aronowski and Zhao, 2011), Wowk et al., unpublished). Superoxide dismutases are endogenous antioxidant enzymes that convert superoxide radicals into O₂ or H₂O₂. Following injection of lysed erythrocytes, manganese superoxide dismutase and

copper-zinc superoxide dismutase levels are depleted, contributing to the high levels of oxidative stress (Wu et al., 2002).

Oxidative stress induced by iron-mediated free radical generation directly causes BBB dysfunction by damaging endothelial cells and activating pathways regulating BBB permeability (*e.g.* those regulating MMP production, tight junction modification) (Pun et al., 2009, Fraser, 2011). Some protective mechanisms exist to defend the BBB against oxidative damage. For example, it has been speculated that elevated Fe leads to increased cysteine uptake in ECs, thereby triggering an antioxidant response that could protect the BBB (Keep, 2008).

1.3.4.4.2 Chloride dyshomeostasis

As the BBB regulates CNS ion homeostasis, BBB dysfunction contributes to alterations in ion concentration after ICH. Chloride homeostasis is maintained in part by the chloride-cation cotransporters, the bumetanide-sensitive $\text{Na}^+\text{-K}^+\text{-2Cl}^-$ cotransporter (NKCC1), which controls chloride influx, and the neuron-specific $\text{K}^+\text{-Cl}^-$ cotransporter-2 (KCC2), which controls chloride efflux. Changes in chloride homeostasis due to alterations in the ratio of the cotransporters impact γ -aminobutyric acid (GABA) signalling polarity and have been noted in many neurological disorders (*e.g.* status epilepticus, spinal cord injury, TBI) (Plotkin et al., 1997, Bonislawski et al., 2007, Silayeva et al., 2015). Downregulation of many chloride transporters is seen as early as 24 hours after ICH (Lu et al., 2006). The downregulation of KCC2 after ISC is associated with both calcium and chloride dyshomeostasis and cell death (Pond et al., 2004). Interestingly, administration of diazepam, a GABA_A receptor agonist, within two hours of oxygen-glucose deprivation *in vitro* can prevent KCC2 downregulation and intracellular chloride

and calcium accumulation, thereby maintaining GABA signalling. Despite this narrow therapeutic window, the authors suggest that diazepam could still be effective outside this period (Galeffi et al., 2004).

KCC2 co-transporters are downregulated after axonal injury, leading to intracellular accumulation of chloride, although NKCC1 receptors are not affected (Shulga et al., 2008). Furthermore, administration of an NKCC1 antagonist, bumetanide, was able to block the intracellular calcium transients associated with depolarization, suggesting that NKCC1 maintains the intracellular chloride accumulation seen after injury (Shulga et al., 2008). By impacting intracellular ion concentrations, NKCC1 and KCC2 expression directly impact glycine and GABA neurotransmission. In mature neurons, chloride influx occurs when GABA binds to the GABA_A receptor, yielding an overall hyperpolarizing inhibitory effect. However, GABA has the opposite effect in immature neurons, causing an outward chloride current, inward calcium current, and depolarization. When this shift in polarization occurs, seizure occurrence is more regular (Nabekura et al., 2002, Gamba, 2005, Shulga et al., 2008). Interestingly, seizures occur in approximately 66% of rodents in the collagenase model, suggesting that this excitatory switch may also occur after ICH (Klahr et al., 2015). Further work must be done to fully elucidate the mechanisms underlying post-ICH seizures in preclinical models.

1.4 Purpose

This thesis has 2 aims, both to be investigated in the collagenase model of ICH. First, the temporal progression of BBB damage will be assessed using spectrophotometry. We

hypothesize that BBB permeability will be highest at day 3 post-ICH and return to naïve tissue levels by day 14. Second, we will establish a novel method to assess the spatial relationship between acute ion dyshomeostasis and BBB dysfunction using XFI to precisely measure elemental concentrations. The latter assessment is the first study to date to use XFI methods in evaluating BBB damage in any stroke model. We hypothesize that there will be high BBB permeability in all samples, and that the degree of BBB permeability will be correlated with ion dyshomeostasis.

Chapter 2: Prolonged blood-brain barrier injury occurs after experimental intracerebral hemorrhage and is acutely associated with ion dyshomeostasis.

2.1 Introduction

An intracerebral hemorrhage (ICH) occurs due to vessel rupture in the brain parenchyma, accounts for 10-15% of all strokes, and has a 40% 1-month mortality rate (Sacco et al., 2009, Flaherty et al., 2010). Approximately 20% of these cases result from anticoagulant use (Flaherty et al., 2010). These anticoagulants, such as warfarin, may transform asymptomatic microhemorrhages into a symptomatic ICH (Leary and Saver, 2003). Indeed, warfarin use increases risk of microbleed transformation into symptomatic (*i.e.* associated with neurological changes and/or death) ICH 80-fold (Lee et al., 2009).

Primary, mechanical damage occurs at ictus when blood from the initial rupture dissects through surrounding tissue (Schlunk and Greenberg, 2015). This is compounded by ischemic injury in the center of the hematoma, where the ruptured and damaged vessels can no longer supply adequate blood to region (Knight et al., 2008). Secondary damage occurs in the perihematoma zone (PHZ) (*i.e.* the region of tissue immediately surrounding the hematoma). Secondary damage is characterized by cell death, oxidative damage, and inflammation. Although the complete set of secondary events and their contributions have not been fully elucidated, the activation of multiple pathways by intraparenchymal blood most likely mediates considerable damage (Aronowski and Zhao, 2011, Schlunk and Greenberg, 2015).

The neurovascular unit (NVU) is a multicellular system composed of endothelial cells (EC), neurons, pericytes, and glial cells that comprises the blood-brain barrier (BBB) to control

the efflux and influx of substances for proper neurotransmission and limit passive diffusion of compounds between the blood and the brain (Siegenthaler et al., 2013, Andreone et al., 2015). Clinically, magnetic resonance imaging of gadolinium-based contrast agents is used to assess BBB permeability and allows spatial assessment of BBB injury with few to no side effects (Montagne et al., 2016). In patients, BBB dysfunction is biphasic. Acute BBB dysfunction occurs during the initial vascular disruption of the hemorrhage, and later dysfunction may be indicative of secondary injury (*e.g.* inflammation) or repair (*e.g.* angiogenesis) processes. Indeed, contrast agent extravasation has been noted in the first 24 hours post-ictus in patients with on-going bleeding, with delayed disruption occurring as well (Murai et al., 1998, Hallevi et al., 2010). In a small prospective study with BBB damage measured approximately 8 days post-ICH, there was high permeability in PHZ, but not hematoma, tissue and low to no BBB damage in the contralateral hemisphere (Aksoy et al., 2013).

BBB injury has been characterized in ICH models. In the collagenase model, BBB permeability is persistently elevated from 5 hours to 7 days post-injection, with function restored by day 14 (Rosenberg et al., 1993). High BBB permeability has been detected in the hematoma, but not PHZ, 12 hours post-collagenase injection, with BBB hyperpermeability increasing to at least day 4 in the hematoma and PHZ (MacLellan et al., 2008). Conversely, the autologous whole blood (AWB) model causes persistently low elevations in BBB permeability in both the hematoma and the surrounding region (Knight et al., 2008, MacLellan et al., 2008). In animal models, Evans blue (EB) dye is commonly used to assess BBB permeability. EB binds to the large molecule albumin and can be quantified in tissue sections visually or using spectrophotometry (Radu and Chernoff, 2013). The collagenase model, despite its limitations,

best mimics clinical BBB damage following ICH at least with regard to the temporal profile of BBB permeability.

After ICH, indirect and direct BBB damage occurs and is characterized by increased permeability due to paracellular and transcellular changes (for review, see (Keep et al., 2014)). This BBB dysfunction is caused by both blood components and secondary injury processes. For example, tight junctions and ECs are disrupted by thrombin (upregulated within 3 hours in animal models) and matrix metalloproteinases (MMPs; upregulated within 1 – 3 days and generated by inflammatory response) (Lee et al., 1997, Lischper et al., 2010, Liu et al., 2010). The degradation of tight junctions facilitates the passage of water-soluble molecules, macromolecules (*e.g.* albumin), ions, and nutrients in the paracellular space and into the parenchyma (Hawkins and Davis, 2005).

This contributes to ion dyshomeostasis after ICH. Such ion dyshomeostasis (*e.g.* alterations in Fe, K⁺, Cl⁻, and Na⁺ levels) occurs within 24 hours of ictus and persists until at least day 28 (Patel et al., 1999, Williamson et al., 2017). Acutely, dyshomeostasis of K⁺, Cl⁻, and Na⁺ can likely be attributed to edema, although K⁺ and Cl⁻ dyshomeostasis persists long after edema is thought to be resolved (*i.e.* after Day 3 in animal models) (Yang et al., 1994, Xu et al., 2015). BBB dysfunction is directly related to edema, as large molecule (*e.g.* albumin) extravasation contributes to vasogenic edema (Schoknecht et al., 2015). Changes in extracellular potassium may also result from alterations in network excitability mediated by astrocyte activation and BBB dysfunction (David et al., 2009). Conversely, iron dyshomeostasis is driven by hematoma resolution. Erythrocyte lysis begins approximately one day after ICH, leading to the release of hemoglobin and subsequent release of redox active iron (Wagner et al., 2003, Chen-Roetling et

al., 2015). Notably, sole injection of blood components, such as lysed erythrocytes, hemoglobin, or iron, all induce BBB dysfunction leading to edema, cell death and behavioral dysfunction (Xi et al., 2001, Katsu et al., 2010, Zhao et al., 2011, Yang et al., 2013).

Iron dyshomeostasis can be assessed using X-ray fluorescence imaging (XFI) (Pushie et al., 2014). In this method, tissue samples are exposed to high energy x-rays, after which the sample will emit characteristic energy spectra that are detected with a specialized detector. Elemental concentrations can then be determined based on emitted wavelengths. This technique is preferred over traditional bulk biochemical assays because it allows for fine spatial resolution and a clear delineation between the hematoma and PHZ. Furthermore, it is considered superior to traditional histochemical stains such as the Perls and Turnbull stains for measuring iron in certain contexts. Perls and Turnbull stains are used to semi-quantitatively measure non-heme iron levels based on the appearance of an insoluble precipitate. Perls stains both ferrous and ferric iron, while Turnbull stains specifically ferrous iron (Meguro et al., 2007). Because most iron is bound to heme until erythrocyte lysis begins, use of these stains are not recommended for early survival times. Furthermore, histochemical stains may damage or dissolve fragile tissue (*e.g.* that in the hematoma) in the staining process. XFI, although it is a more costly method requiring careful sample preparation, is preferred here because it can measure total element content acutely after ICH (Hackett et al., 2015). XFI has been used in ICH previously (Auriat et al., 2012, Zheng et al., 2012, Hackett et al., 2015, Karuppagounder et al., 2016, Williamson et al., 2017).

We propose a novel method, combining clinical and experimental techniques, to assess BBB injury after ICH. Because gadolinium (Gd) concentration can be determined using XFI, we

will use a gadolinium-based contrast agent and XFI to measure gadolinium extravasation after ICH. This method will allow for detailed insight into the spatial progression of BBB damage after ICH, while allowing us to directly relate BBB permeability with PHZ ion dyshomeostasis. While others have measured gadolinium with synchrotron techniques to assess various pathologies, we are the first to do so in a rodent model of stroke (Le Duc et al., 2000, George et al., 2010, Gastaldo et al., 2011).

Here, the temporal progression of BBB damage was assessed using spectrophotometry. In the collagenase model, acute BBB permeability occurs, with function restored by two weeks. (Rosenberg et al., 1993). Accordingly, we hypothesized that BBB permeability will be highest at day 3 post-ICH and return to naïve tissue levels by day 14. Subsequently, we evaluated the extent of ion dyshomeostasis and BBB dysfunction in the PHZ and then investigated the spatial relationship between acute ion dyshomeostasis and gadolinium extravasation using XFI. The latter assessment is the first study to date to use XFI methods to evaluate BBB damage in any stroke model. Ion dyshomeostasis has been noted as early as 24 hours post-ictus (Patel et al., 1999). As XFI will be used acutely (*i.e.* 72 hours) after ICH, we hypothesized that there will be high ion dyshomeostasis and BBB permeability in all ICH samples, and that the degree of BBB permeability will be correlated with ion dyshomeostasis.

2.2 Materials and Methods

2.2.1 Subjects

All procedures conform to the Canadian Council of Animal Care Guidelines and were approved by the Animal Care and Use Committee for Biosciences at the University of Alberta. Seventy-two male Sprague-Dawley rats (350-450 g) were obtained from Charles River (Saint Constant, QC). Food and water were provided ad libitum, and rats were individually housed in a temperature- and humidity-controlled room with a 12-hour light cycle.

2.2.2 Experiment 1

Experimental Groups

Animals were randomly assigned to either the sham surgery (SHAM) or collagenase groups prior to surgery (n=5 SHAM; n=36 collagenase). Previous research in our lab indicates low variability in EB concentration in SHAM animals; thus, lower numbers were used in this group (MacLellan et al., 2006b). Collagenase animals were then randomly assigned to either the three day (3D; n=13), seven day (7D; n=13), or 14 day (14D; n=10) survival groups.

Intracerebral Hemorrhage

A collagenase model of ICH was used (Rosenberg et al., 1993). Rats were anesthetized using isoflurane gas (4% induction; 2% maintenance; 60% N₂O, remainder O₂) for aseptic surgery. The head was shaved and disinfected with 70% ethanol and betadine, and 0.1 mL of Marcaine (bupivacaine hydrochloride; Hospira, Saint-Laurent, QC) was injected subcutaneously. After a midline incision was made, a burr hole was drilled 0.5 mm anterior and 3.5 mm left of Bregma. A 26-gauge Hamilton syringe (Hamilton, Reno, NV, USA) was lowered 6.5 mm into the striatum, and 0.14 U of bacterial collagenase (Type IV-S; Sigma, Oakville, ON, Canada) was injected over 5 minutes. The needle was withdrawn 5 minutes after completion of the injection,

and then a screw (model MN-0080-02P-25; Small Parts Inc., Miami Lakes, FL, US) was put in place to seal the hole. The wound was then closed with staples after application of Marcaine at the incision site. Body temperature was maintained for the duration of surgery (~30 minutes) using a rectal temperature probe and warm water blanket. For SHAM surgeries, animals underwent similar procedures, but, after the midline incision was made, were kept under anaesthesia for the same amount of time as an average collagenase surgery. The incision was then closed using the same methods as the collagenase surgery.

Evans Blue Spectroscopic Assay

Evans blue extravasation was assessed as done previously (MacLellan et al., 2006b). Evans blue dye (Sigma; 2% in saline; 4 mL/kg; filter sterilized) was injected into the tail vein. Injection success was confirmed visually. Dye circulated two hours before rats were transcardially perfused with saline. The brain was extracted, and each hemisphere (ipsilateral, IPSI; contralateral; CONTRA) was homogenized in 0.1 M PBS. The sample was centrifuged, and the supernatant was incubated at 4 °C with trichloroacetic acid (50% w/v; Fisher Scientific, Whitby, ON) and centrifuged. The absorbance was read at 610 nm. Thirteen additional rats were used to generate a standard curve with known amounts of dye (0.2 to 1.0 µL) added to naïve tissue from which the amount of Evans blue extravasation was calculated.

2.2.3 Experiment 2

Experimental Groups

Rats were given collagenase or SHAM surgeries as described in experiment 1 and euthanized 72 hours later. Four animals were assigned to SHAM (n=2), and collagenase (n=2),

for inductively-coupled mass spectrometry (ICPMS) analysis. Ten additional animals were then assigned to SHAM (n=5) or collagenase (n=5) surgery groups for XFI analysis

Magnevist® Injections

Magnevist® (gadopentetate dimeglumine; 2.5 mL/kg; Bayer, Mississauga, ON) was injected into the tail vein and allowed to circulate for 10 minutes due to its short half-life in rats and previous research (Le Duc et al., 2004, Dohanish et al., 2009). Rats were then decapitated and brains were removed in 2 minutes or less. For XFI, brains were rapidly frozen in cooled isopentane.

Inductively-Coupled Plasma Mass Spectrometry (ICPMS)

As synchrotron analysis of BBB injury using gadolinium-based contrast agents is novel, ICPMS was first performed to quantify gadolinium levels and ensure adequate gadolinium remained in the brain 10 min after intravenous infusion. Brains for ICPMS were divided into hemispheres. Each hemisphere was digested in 5 mL of nitric acid (Fisher Scientific, Edmonton, AB) over seven days. Samples were measured with an ICAP-Q quadrupole ICPMS (Thermo Scientific) at the Canadian Centre for Isotopic Microanalysis. Average gadolinium concentration for whole CONTRA, IPSI, and SHAM hemispheres was then calculated.

X-Ray Fluorescence Imaging (XFI)

We took 20 µm tissue sections that were mounted on metal-free Thermanox coverslips (Thermo Scientific, Waltham, MA). Data were collected at the Stanford Synchrotron Radiation Lightsource (SSRL) at beamline 10-2 as described previously (Williamson et al., 2017). Briefly,

maps of Ca, Cl, Cu, Fe, Mn, K, Zn, and Gd were collected. Tissue was exposed to a 13450 eV X-ray beam for Ca, Cl, Cu, Fe, Mn, K, and Zn and to a 7700 eV X-ray beam for Gd for 200 ms per 30 μm step and detected with a 35 μm aperture. Emission spectra were collected from standards for all elements. Sam's Microprobe Analysis Kit (SMAK; version 1.3) was used to quantify channels.

Data were reformatted with custom software for use in ImageJ (version 1.50b, National Institutes of Health, Bethesda, MD). Elemental concentrations were determined for the CONTRA striatum, IPSI hematoma, and both striatum for SHAM samples. The hematoma border is where there is a sharp change in Fe, indicating a transition from blood (hematoma) to tissue (PHZ) (Williamson et al., 2017). The hematoma border was estimated in ImageJ using the Fe channel by determining the value for Fe corresponding to the hematoma edge. This threshold was then consistently applied to all samples. The hematoma border was applied to all element channels in a given sample. ROIs were taken for distance analyses for Gd, Fe, Cl, and K and were performed from the hematoma edge to 1260 μm medially, laterally, and dorsally, and all ROIs were averaged together in 180 \times 180 μm bins. Hematoma and PHZ averages for each animal were used to calculate the relationship between Gd and Fe, Cl, and K. Gd was also correlated with Fe, Cl, and K averages every 180 μm into the PHZ. Due to the small sample size, we performed additional exploratory analyses to investigate how the predictive value of Gd concentration on ion dyshomeostasis changes with distance into the PHZ. R^2 values were determined, for each sample, for the relationship between Gd and Cl, Fe, and K within 180 \times 180 μm sections from the hematoma edge into the PHZ. Here, measurements of 30 \times 180 μm

sections in each ROI were included, resulting in 18 measurements for each sample in any given 180 × 180 μm bin.

2.2.4 Statistical Analysis

Data were analyzed using GraphPad Prism (v. 6.0, GraphPad Software Inc., La Jolla, CA). Two-way ANOVAs were used in experiment 1 to assess time x hemisphere effects. One-tailed Student's t-tests were performed to assess differences in CONTRA permeability across days. These tests were used to determine if there were any trends in the CONTRA hemisphere, as our planned analyses were underpowered to detect the changes noted in experiment 1. One-tailed tests were used because high permeability has been noted in past work. One-way ANOVAs were used in experiment 2 to assess region effects. Repeated measures ANOVA was used to assess distance main effects. Hematoma values were not included in distance analyses. Bonferroni post-hoc tests were used in both experiments 1 and 2 to control Type II error. Bartlett's tests were used to assess assumptions of equal variance. If variance was not equal, Kruskal-Wallis tests were used. Proportions in experiment 1 were compared with a Chi-squared test. Statistical significance was defined as $P < 0.05$. All data are presented as mean ± standard deviation (SD).

2.3 Results

Mortality and Exclusions

All animals tolerated the surgery well; there were no mortalities. In experiment 1, one SHAM sample was excluded from analysis due to incomplete perfusion. In experiment 2, two SHAM samples were not imaged due to time constraints at SSRL.

Experiment 1

Blood-brain Barrier Permeability Is Highest at Day 3 and Decreases Thereafter

A two-way ANOVA was performed to evaluate the relationship between time and hemispheric BBB extravasation. There was a main effect of day ($P < 0.001$) and of hemisphere ($P < 0.001$), with greater EB extravasation in the IPSI hemisphere compared to CONTRA. Bonferroni post-hoc tests revealed ipsilateral 3D BBB permeability was significantly higher than D7 ($P < 0.01$), D14 ($P < 0.001$), and SHAM (Figure 2-1A; $P < 0.001$). D7 IPSI BBB permeability was higher than SHAM ($P < 0.05$). There were no differences in BBB permeability between groups in the CONTRA hemisphere, although BBB permeability was higher than expected. Therefore, to discern any trends in the data, we tested CONTRA values against SHAM values at each time using a one-tailed Student's t-test. Interestingly, CONTRA 3D, 7D, and 14D BBB permeability was significantly higher than SHAM values when these tests were run ($P = 0.02$, $P = 0.03$, and $P = 0.01$, respectively). These tests revealed no significant differences between days in the CONTRA hemisphere ($P > 0.05$).

A Subset of Animals Display BBB Dysfunction

High variability was noted in the data (Figure 2-1B). BBB hyperpermeability was then categorized as any sample with EB extravasation above that of the highest SHAM level. In the IPSI hemisphere, 100%, 69.2%, and 40% of animals displayed hyperpermeability at days 3, 7,

and 14, respectively. In CONTRA samples, 23.1%, 46.2%, and 40% displayed hyperpermeability at days 3, 7, and 14, respectively. A Chi-square test revealed there is a significant relationship between day post-ICH and BBB permeability in the IPSI ($P < 0.01$), but not CONTRA ($P = 0.451$) (Figure 2-1C).

Experiment 2

ICPMS analysis revealed that Gd could be detected in the brains of collagenase and SHAM operated animals when a dose of 2.5 mL/kg of Magnevist was injected in the tail vein and allowed to circulate for 10 minutes (data not shown). Thus, we proceeded with our XFI data collection. As previously mentioned, XFI allows accurate definition of the hematoma boundary and spatial distribution of injury (Figures 2-2A-D). Cresyl violet staining of the same sections, however, appears to have damaged/destroyed the fragile tissue in the hematoma, and the spatial distribution of BBB permeability and ion dyshomeostasis is impossible to discern (Figure 2-2E). The pattern of injury shown in Figures 2-2A-D was consistent across all ICH samples.

Intracerebral Hemorrhage Induces Ion Dyshomeostasis in the Hematoma and Perihematoma Zone

One-way ANOVA was used to assess changes in element concentration within hematoma of IPSI samples and striatum of CONTRA and SHAM samples. Concentrations of Cl, Fe, Gd, and Mn were significantly increased in the IPSI hematoma as compared to the CONTRA striatum ($P < 0.001$, $P < 0.01$, $P < 0.01$, $P < 0.001$, respectively) and SHAM striatum (Figure 2-3; $P < 0.001$, $P < 0.001$, $P < 0.05$, $P < 0.001$, respectively). IPSI K was significantly decreased below levels in the CONTRA striatum ($P < 0.001$) and SHAM ($P < 0.001$) group. There were no differences in Ca,

Cu, or Zn concentrations across groups ($P > 0.05$). One outlier was noted in the CONTRA group for Cu, but was not excluded.

Repeated measures ANOVAs were used to assess changes in ion homeostasis in the PHZ. Gd was highest in the hematoma and was significantly different from SHAM and CONTRA values from 0 – 360 μm into the PHZ (Figures 2-3A and 2-4A; $P < 0.001$, distance main effect). It appeared there was little Gd in the center of the hematoma, with high Gd concentrations closer to the hematoma edge (Figure 2-2A). Fe was highest in the hematoma and was significantly higher than SHAM and CONTRA values from 0 – 360 μm into the PHZ (Figures 2-3D and 2-4B; $P < 0.001$, distance main effect). High Fe concentration was noted inside the hematoma boundary (Figure 2-2B). Cl concentrations appeared relatively constant in the hematoma (Figure 2-2C). Cl was highest at the hematoma border, and levels normalized after 360 μm into the PHZ (Figures 2-3B and 2-4C; $P < 0.001$, distance main effect). K concentrations in the hematoma appeared relatively constant, although a ring of slightly higher concentration was observed closer to the hematoma edge (Figure 2-2D). K was lowest at the hematoma border and was significantly lower than CONTRA and SHAM values from 0 – 360 and 0 – 720 μm into the PHZ, respectively (Figures 2-3F and 2-4D; $P < 0.001$, distance main effect).

Blood-brain Barrier Permeability Is Associated with Ion Dyshomeostasis in the Perihematoma Zone, but Not the Hematoma

Gd was not significantly correlated with any of the measured elements in the hematoma except Mn (Table 2-1) ($r = 0.989$; $P = 0.001$). Average Gd was then correlated in the PHZ with average Fe, K, and Cl (Tables 2-1 and 2-2). In the PHZ, Gd was correlated with Cl and K from 901

– 1260 μm into the PHZ (Table 2-2). Interestingly, all correlations were positive in the hematoma and PHZ except that with Fe, although the correlations with Fe were non-significant.

Our exploratory analyses revealed that Gd was significantly correlated with Cl and K in many samples from 0 – 900 μm (Figure 2-5A and C). Despite this, it appears that Gd concentration has low and/or variable predictive value for Cl and K concentration. The proportion of Cl and K variance accounted for by Gd concentration does not change with distance from the hematoma edge. Gd concentration was significantly correlated with Fe concentration in the majority of samples from 0 – 720 μm (Figure 2-5B). Gd concentration appears to account for a large proportion of Fe variance close to the hematoma/PHZ interface, with this effect lessening with distance into the PHZ.

2.4 Discussion

BBB injury occurs following ICH and is related to many other forms of secondary injury (*e.g.* edema, inflammatory response). We found that BBB permeability was highest in the IPSI hemisphere and decreased with time. Here, we present the novel and successful use of XFI to measure BBB permeability using a gadolinium-based contrast agent. We established a novel method that provides a fine spatial resolution to both measure the extent of BBB dysfunction and to co-localize these changes with various elements. Using this novel method, as well as a commonly used Evans Blue assay, we confirm and expand upon the nature and progression of BBB injury in the collagenase model of ICH at various survival times. We are the first to

investigate the magnitude of ion dyshomeostasis and BBB dysfunction in the PHZ 3 days post-ICH.

We found that ipsilateral BBB permeability peaked 3 days after ICH and decreased thereafter, with most injury resolved within 2 weeks of injury. Interestingly, we noted a trend in contralateral BBB permeability, where there was greater permeability at days 3, 7, and 14 after ICH compared to sham tissue. Importantly, we noted high variability in BBB permeability in both hemispheres at all times measured, which could indicate a variety of underlying injury (*e.g.* inflammation) and repair (*e.g.* angiogenesis) mechanisms. In accordance with data from our EB assay, we showed, using novel methodology, that there is high acute BBB permeability. This BBB permeability is related to ion dyshomeostasis in the PHZ, but not the hematoma.

We observed that approximately 70% and 40% of animals displayed ipsilateral BBB hyperpermeability at days 7 and 14, respectively, using an Evans Blue spectrophotometric assay. Furthermore, contralateral BBB hyperpermeability incidence increased from approximately 20% on day 3 to 40% on day 14 post-ICH, although this was not significant. We propose that these changes may indicate late angiogenesis or disrupted vascular integrity (*i.e.* due to microbleeds). Indeed, delayed changes in the NVU, including the BBB, often indicate a shift from injury to repair because it facilitates angiogenesis and other processes (Arai et al., 2009). Changes in vessel density, indicating angiogenesis, are observed between days 7 and 14 post-ICH in the collagenase model (Lei et al., 2015). Conversely, the observed variability may represent disrupted vasculature. At day 3, 100% of animals showed hyperpermeability.

Neutrophil response in the PHZ begins within 4 hours of ictus and peaks between 2 to 3 days later, leading to elevated levels of MMPs (Gong et al., 2000, Xue and Del Bigio, 2000, Wang and

Dore, 2007). MMPs contribute to BBB dysfunction by degrading tight junctions *in vitro* and in ischemic stroke models, and, therefore, may contribute to the acute injury observed here (Yang et al., 2007, Lischper et al., 2010, Yang and Rosenberg, 2011). At later time points, MMP-9 may contribute to microhemorrhaging, as MMP-9 degrades the basal lamina of vessels, thereby weakening vessels and making them more vulnerable to rupture and subsequent microhemorrhaging (Gasche et al., 1999, Gidday et al., 2005). Overexpression of MMP-9 has been noted at day 7 in patients and animal models, a time when relatively high BBB dysfunction was observed (Power et al., 2003, Castellazzi et al., 2010). Notably, collagenase (used for this model) is MMP-9, so it is possible that there are low but enduring effects of injection of this compound. Although elevations in MMP-9 expression have been noted as late as day 14 in the collagenase model of ICH, no one has yet assessed this in the AWB model, making it difficult to understand the contributions of exogenous versus endogenous MMP-9 to these changes (Chang et al., 2014).

Using XFI, we report that Cl, Fe, K, and Mn were altered in the hematoma after ICH. In accordance with our EB data, as well as magnetic resonance imaging studies, XFI revealed high BBB permeability (measured by Gd concentration) in the ipsilateral hemisphere acutely after ICH (Knight et al., 2008, MacLellan et al., 2008, Aksoy et al., 2013). Interestingly, we note that there was very little Gd in the center of the hematoma. As ischemia occurs in the hematoma, it is likely that there was inadequate vasculature and/or blood supply to deliver Gd to that area (Knight et al., 2008). This likely explains why Gd was not correlated with most elements in the hematoma. We found that, for gadolinium, iron, chloride, and potassium, the greatest ion dyshomeostasis occurred at the hematoma/PHZ interface and normalized with distance into

the PHZ. We found that BBB dysfunction and the associated iron and chloride ion dyshomeostasis did not extend far into the PHZ (~360 μm), while potassium dyshomeostasis extended to at least 720 μm into the PHZ. Similar changes (*i.e.* a gradient of ion dyshomeostasis) have been noted in our previous work (Williamson et al., 2017). It appears that ion dyshomeostasis matures, impacting tissue further into the PHZ over time. This may be related to ongoing injury in the region. For example, progressive cell death begins within 24 hours of ICH in the PHZ, with apoptotic processes resolved within a week (Felberg et al., 2002). Cell death, ion dyshomeostasis, and other processes likely contribute to the ongoing behavioral dysfunctions observed acutely following experimental and clinical ICH (Jorgensen et al., 1999, MacLellan et al., 2008).

We also report that BBB injury was significantly correlated with these ionic gradients in the PHZ to varying degrees. Under normal physiological conditions, the BBB maintains ion levels (*e.g.* Na^+ , Cl^- , K^+) (Abbott et al., 2010). At day 3 post-ICH, we found that BBB injury only extended approximately 360 μm into the PHZ. Despite this, BBB permeability, as measured by Gd concentrations, was correlated with iron, potassium, and chloride further from the hematoma edge in the PHZ. Thus, it is possible that BBB dysfunction contributes to persistent, diffuse ionic imbalances in the early stages after ICH, either alongside or independently of ongoing injury in the region. The positive correlation between Gd, Cl, and K is likely indicative of perihematoma edema, which is known to peak between days 1 and 3 in this model (Chang et al., 2014). Interestingly, Gd and Fe were negatively correlated, in two samples, in 180 x 180 μm increments as far as 720 μm from the hematoma/PHZ edge. This may indicate that the presence of microbleeds in the ipsilateral hemisphere, as areas with blood deposition (*i.e.* high

iron) would have damaged vasculature that is no longer functional, thus preventing the later deposition of Gd. Conversely, high Fe levels are associated with high edema (Huang et al., 2002) and may lead to the dilution/diffusion of any extravasated Gd.

As expected, iron dyshomeostasis was noted. Others have found PHZ iron accumulation at 24 hours post-ICH using a similar method (Auriat et al., 2012) and with more traditional methods (*i.e.* Perls stain) (Wu et al., 2011). In patients and in animal models, iron toxicity negatively contributes to functional outcome (Perez de la Ossa et al., 2010, Wu et al., 2011). Iron accumulation after ICH is primarily a result of erythrocyte lysis. Iron was highest at the hematoma/PHZ interface and concentrations normalized with distance. This likely contributes to lesion expansion. Progressive lesion expansion and tissue damage occurs after ICH in the collagenase model (MacLellan et al., 2008, Nguyen et al., 2008). Thus, tissue closer to the hematoma experiences greater damage than distal structures, with more tissue impacted over time (Felberg et al., 2002). Interestingly, we found low Fe levels in the center of the hematoma in all ICH animals and a ring of high concentration close to the hematoma edge. Microglia and macrophages expressing the CD163 receptor, which facilitates hemoglobin endocytosis, localize at the PHZ/hematoma edge within 3 days of ICH and infiltrate the hematoma with time (Cao et al., 2016). Therefore, the high concentrations of iron observed at the hematoma edge here may represent a summation of both iron in the hematoma itself and iron internalized by microglia/macrophages (*i.e.* that present in hemoglobin). Thus, this band of cells may grow in size or intensity with time as more Hb and Fe are accumulated.

Iron dyshomeostasis in the PHZ likely impairs neural function and functional outcome, although this has not yet been studied in ICH. Early injury to PHZ neurons and dendrites has

been noted in ICH, and this injury may be a result or cause of the observed changes in ion concentrations (Nguyen et al., 2008). Chloride homeostasis is maintained, in part, by the chloride-cation cotransporters: the bumetanide-sensitive Na-K-2Cl cotransporter (NKCC1) and the neuron-specific K⁺-Cl⁻ cotransporter-2 (KCC2). Alterations in the ratio of these cotransporters disrupt Cl⁻ homeostasis and cause a shift in γ -aminobutyric acid (GABA) signalling polarity, a phenomenon noted in many neurological disorders (*e.g.* status epilepticus, spinal cord injury, traumatic brain injury) (Plotkin et al., 1997, Bonislowski et al., 2007, Silayeva et al., 2015). When this shift in polarization occurs, seizure occurrence is more regular (Nabekura et al., 2002, Gamba, 2005, Shulga et al., 2008). Interestingly, seizures occur in approximately 66% of rodents in the collagenase model of ICH within 3 days of stroke, suggesting that this excitatory switch in GABA occurs acutely after stroke as well (Klahr et al., 2015, Klahr et al., 2016). In ischemic stroke, reversal of GABA polarity is initially neuroprotective, but later hampers recovery (Carmichael, 2012). In light of these considerations, future research should determine whether the chloride dyshomeostasis observed here is intra- or extra-cellular.

We found that BBB permeability, as measured by Gd concentration, was significantly correlated with K in the PHZ. Furthermore, we found that K⁺ concentrations are locally decreased after ICH and normalize with distance into the PHZ. This association is likely mediated by alterations in astrocytes after ICH. Astrocytes are important for maintenance of K⁺ homeostasis and are an important component of the NVU. Astrocytes clear excess extracellular K⁺ through *K⁺ spatial buffering* (Gardner-Medwin, 1983, Kofuji and Newman, 2004). Alternatively, excess extracellular K⁺ and Cl⁻ can be stored in astrocytes, although this can

contribute to edema (Walz, 2000). After ICH, astrocytes are activated in the PHZ within 72 hours, with elevated astrocyte numbers persisting to at least day 14 (Wang and Dore, 2008, Caliaperumal and Colbourne, 2014). Interestingly, astrocyte activation decreases from the hematoma edge into the PHZ (Wang, 2010). Here, we report that K^+ is decreased in the PHZ and normalizes with distance from the hematoma 72 hours post-ICH, while others report similar findings at Day 14 (Williamson et al., 2017). Considering the role astrocytes play in regulating potassium homeostasis, it is possible that the elevation in astrocyte numbers contributes to the observed decrease in PHZ potassium concentrations. Future work should assess where the K dyshomeostasis occurs (*e.g.* in neurons, astrocytes, extra- or intra-cellularly) as we were unable to discern this with XFI.

Limitations and Future Directions

This work is not without limitations. First, we only measured BBB permeability to large molecules (~55-60 kDa). Importantly, the BBB may open to large molecules while still restricting movement of small ions and vice versa, so future experiments will assess the temporal progression of BBB permeability to small molecules and compare to what is described here (Kang et al., 2013). Second, XFI cannot be used to determine the chemical state of iron. Thus, we cannot discern whether iron is toxic. In addition, because the L-edge of Gd is close to iron, it is possible that Gd signal is partially contaminated by that of Fe and vice versa. Furthermore, because we used non-perfused tissue, Fe and Gd are present in the vasculature. It was important to prepare our tissue this way, however, to avoid introducing artifacts. In addition, we were unable to measure changes in Na with XFI using our specified parameters and equipment. Moreover, we were unable to elucidate a causal relationship between BBB damage

and ion dyshomeostasis. Finally, functional significance of the described changes was not assessed. As previously mentioned, there are many structural abnormalities in the PHZ, such as those noted in Golgi-Cox stained neurons, that resolve with time (Nguyen et al., 2008). These acute structural changes, in conjunction with ion dyshomeostasis, may contribute to the high seizure incidence and behavioral impairments that have been noted by others (MacLellan et al., 2006a, Klahr et al., 2015). Future studies will examine the mechanisms underlying the variability in BBB permeability observed after ICH. Also, we will evaluate the short- and long-term behavioral effects of acute ion dyshomeostasis.

2.5 Conclusions

Here, we present a novel, spatially-sensitive technique to concurrently assess BBB permeability and ion dyshomeostasis using a gadolinium-based contrast agent and XFI. We show that both persistent BBB injury and acute ion dyshomeostasis occurs after ICH. The observed dyshomeostasis is related to BBB dysfunction in the perihematoma, but not hematoma, zone. Further understanding of these changes could aid in the development of acute treatments for ICH by providing further insights into the mechanisms underlying injury and functional impairments.

CHAPTER 3

3.1 Primary findings

The purpose of this thesis was to measure changes in BBB permeability over time and assess the relationship between BBB permeability and acute ion dyshomeostasis in a rat model of collagenase-induced ICH. In experiment 1, we measured Evans Blue extravasation, a marker of BBB permeability to the macromolecule albumin, at D3, D7, and D14 after ICH. We found that BBB injury was initially high and decreased by D14, but that there was high variability at all times assessed. We evaluated the magnitude and extent of BBB dysfunction and ion dyshomeostasis in the hematoma and PHZ. We then assessed the relationship between BBB permeability and ion dyshomeostasis at 3 days post-ICH, a time when almost all animals displayed hyperpermeability in experiment 1, using a novel method. We demonstrated that ion dyshomeostasis occurs and is correlated with BBB injury in the PHZ. Taken together, this work yields four main conclusions: a) early BBB injury is severe and dysfunction may persist to day 14 post-ICH or longer, b) there is a relationship between time and incidence of BBB hyperpermeability, c) XFI can be used to simultaneously measure BBB integrity and ion dyshomeostasis, and d) acute ion dyshomeostasis and BBB dysfunction occur in the hematoma and PHZ.

3.2 Blood-brain barrier permeability is highest at day 3 and decreases thereafter

In experiment 1, we assessed the temporal progression of BBB permeability by measuring Evans Blue extravasation at 3, 7 and 14 days after collagenase ICH. We found that

BBB permeability was significantly higher on days 3 and 7 in the ipsilateral hemisphere as compared to SHAM. Peak BBB permeability was on day 3, and there was no significant difference between day 14 and SHAM. Importantly, 40% of animals displayed BBB dysfunction at day 14 in both hemispheres, indicating that there may be persistent changes in BBB permeability enduring at least two weeks after stroke that could be related to injury or repair processes. Exploratory one-tailed t-tests indicate contralateral BBB permeability is higher than sham tissue at all survival times. Unfortunately, this research was underpowered to detect an effect of this size with our planned analyses, as power calculations indicate a sample size of 16 per group would have been needed.

These findings confirm and build upon past work by including multiple survival times. Rosenberg and colleagues found that BBB dysfunction is slightly chronically elevated from 5 hours to 7 days post-injection, with BBB function restored by day 14 in the collagenase model (Rosenberg et al., 1993). The temporal progression of BBB injury follows that of other secondary injury processes. For example, BBB disruption is known to precede edema formation (Keep et al., 2014). Peak edema, in the collagenase model, occurs at day 3, a time when we observed very high levels of BBB damage. Furthermore, although hematoma resolution and subsequent erythrocyte lysis begins within 24 hours of ICH, HO-1, the enzyme responsible for hemoglobin breakdown, peaks within 72 hours of ICH (Wagner et al., 2003, Wu et al., 2003). As injection of sole injection of blood components (*e.g.* lysed erythrocytes, hemoglobin, iron) all induce BBB dysfunction, it is logical that there is high BBB injury at day 3 (Xi et al., 2001, Katsu et al., 2010, Zhao et al., 2011, Yang et al., 2013). Finally, neutrophil response in the PHZ begins within 4 hours of ictus and peaks between 2 to 3 days later, leading to elevated levels of MMPs

(Gong et al., 2000, Xue and Del Bigio, 2000, Wang and Dore, 2007). MMPs contribute to BBB dysfunction by degrading tight junctions *in vitro* and in ischemic stroke models and are likely contributing to the acute injury we observed (Yang et al., 2007, Lischper et al., 2010, Yang and Rosenberg, 2011). It is likely that BBB damage resolves as these processes decline.

3.3 Blood-brain barrier injury varies between subjects and time

Variability in Evans Blue extravasation was noted at days 3, 7, and 14 in the ipsilateral hemisphere. Hyperpermeability, indicating high BBB dysfunction, was then categorized as any value above the highest SHAM value. We demonstrated that there is a significant relationship between hyperpermeability incidence and time in the ipsilateral, but not contralateral, hemisphere.

Acute BBB hyperpermeability was expected, as outlined above. However, we observed that approximately 70% and 40% of animals displayed ipsilateral BBB dysfunction at days 7 and 14, respectively. This subset may represent animals undergoing considerable angiogenesis or perhaps delayed vascular injury. BBB injury is biphasic, with acute damage attributed to mechanical vessel damage and activation of inflammatory response, among others (Fisher, 2008). Delayed BBB permeability, on the other hand may indicate a shift from injury to repair by facilitating angiogenesis and other repair processes (Arai et al., 2009). Changes in vessel density, indicating angiogenesis, are observed between days 7 and 14 post-ICH in the collagenase model; however, the spatiotemporal progression of angiogenesis after ICH has not been fully determined (Lei et al., 2015). VEGF is upregulated after ICH, and VEGF-labelled

microvessels begin to be detected at day 7 in the PHZ (Tang et al., 2007). Thus, the variability seen on day 7 may be attributed to the beginning of angiogenesis-related processes.

Conversely, the observed variability may represent disrupted vasculature due to MMP-9 activity and oxidative stress. Oxidative stress occurs following ICH due to free radical generation by the inflammatory response and iron release following erythrocyte lysis (Duan et al., 2016). Oxidative stress can upregulate MMP activity and contributes to microbleed occurrence (Toth et al., 2015). MMP-9 may induce microhemorrhaging by degrading the basal lamina of vessels, thereby weakening vessels and making them more vulnerable to rupture and subsequent microhemorrhaging (Gasche et al., 1999, Gidday et al., 2005). Overexpression of MMP-9 has been noted at day 7 in patients and animal models, a time when relatively high hyperpermeability was observed (Power et al., 2003, Castellazzi et al., 2010). Therefore, the observed BBB dysfunction may be indicative of microhemorrhages.

3.4 Acute ion dyshomeostasis occurs after intracerebral hemorrhage

In experiment 2, we developed novel methods to spatially assess BBB permeability. Animals were given collagenase-induced ICH and euthanized at day 3, a time when high hyperpermeability was noted, after injection with a clinically-used gadolinium-based contrast agent. We then measured extravasation of gadolinium and other elements using XFI. We noted ion dyshomeostasis in the hematoma and perihematoma zones, with Cl, Fe, and K dyshomeostasis normalizing with distance into the PHZ. There were high Gd concentrations,

indicating BBB permeability, in the hematoma and in the PHZ close to the hematoma edge. Interestingly, BBB permeability was related to PHZ, but not hematoma, ion dyshomeostasis.

Others have measured gadolinium extravasation using magnetic resonance imaging and found that, on day 4, BBB damage in the hematoma and PHZ zones was significantly higher in the collagenase model compared to the AWB model (MacLellan et al., 2008). Our finding, that BBB permeability is significantly increased in these regions at day 3 using XFI, is in line with previous work and validates the use of this novel method. XFI and other synchrotron techniques have previously been used to spatially map ICH-induced iron dyshomeostasis. Iron dyshomeostasis in the hematoma has been noted within 24 hours of ICH, with perihematomal dyshomeostasis occurring from days 1 – 21 (Auriat et al., 2012, Zheng et al., 2012, Hackett et al., 2015, Williamson et al., 2017). Others have used this method to assess therapeutic interventions in ISC and ICH (Silasi et al., 2012, Wowk et al., 2016). In accordance, we found that iron concentration is significantly increased in the PHZ and hematoma zones as compared to contralateral and control samples. Overall, this work builds upon the aforementioned research by providing a new method of spatially assessing BBB integrity and contributing to our knowledge of ion dyshomeostasis after ICH. Furthermore, it provides insight into the nature of BBB injury following ICH and points to possible mechanisms underlying the observed variability.

Under normal physiological conditions, the BBB maintains ion levels (*e.g.* Na⁺, Cl⁻, K⁺) (Abbott et al., 2010). At day 3 post-ICH, we found that BBB injury only extended approximately 360 μm into the PHZ. Despite this, BBB permeability, as measured by Gd concentrations, was related to iron, potassium, and chloride levels further from the hematoma edge in the PHZ. Thus, it is possible that BBB dysfunction contributes to persistent, diffuse ionic imbalances in

the early stages after ICH, even before progressive tissue damage begins. The positive correlation between Gd, Cl, and K is likely indicative of perihematomal edema, which is known to peak between days 1 and 3 in this model (Chang et al., 2014). Perihematomal edema is a valuable prognostic tool for clinical ICH, as perihematomal edema growth early after ICH is associated with poor functional outcome (Yang et al., 2015, Urday et al., 2016). This growth may, however, be mediated by hematoma size and severity. Interestingly, Gd and Fe were negatively correlated across the PHZ, although this was not significant. This may indicate that the presence of microbleeds in the ipsilateral hemisphere, as areas with blood deposition (*i.e.* high iron) would have damaged vasculature that is no longer functional, thus preventing the later deposition of Gd.

There was a region in the center of the hematoma of low Gd concentration. This is likely because there are relatively few vessels remaining after blood dissects through tissue in the region, creating an ischemic environment (Knight et al., 2008). There was no correlation between Gd and most elements in the hematoma, likely due to this reason as well.

The imbalances in chloride homeostasis observed here could reflect abnormal cell function and mediate injury. For example, in spinal cord injury, these disruptions are associated with functional impairments such as hyperreflexia (Cote et al., 2014). Chloride dyshomeostasis is associated with a shift in GABA signalling polarity. When this shift in polarization occurs, seizure occurrence is more regular (Nabekura et al., 2002, Gamba, 2005, Shulga et al., 2008). Interestingly, seizures occur in approximately 66% of rodents in the collagenase model within 3 days of ICH, suggesting that this excitatory switch occurs after stroke as well (Klahr et al., 2015). In ischemic stroke, reversal of GABA polarity is initially neuroprotective, but later hampers

recovery (Carmichael, 2012). Others have found that chloride dyshomeostasis persists to at least two weeks after ICH (Williamson et al., 2017). As most seizures occur early, not late, after ICH, it could be that chronic ion dyshomeostasis and/or reversal in GABA polarity is actually protective (Bogousslavsky et al., 1988, Bladin et al., 2000). In accordance, future research needs to first address whether chloride is intra- or extra-cellular using XFI with finer spatial resolution or with electrophysiology.

Chloride homeostasis is maintained, in part, by the chloride-cation cotransporters, the bumetanide-sensitive Na-K-2Cl cotransporter (NKCC1) and the neuron-specific K⁺-Cl⁻ cotransporter-2 (KCC2). Alterations in the ratio of these cotransporters disrupt Cl⁻ homeostasis and impact γ -aminobutyric acid (GABA) signalling polarity. While GABA is inhibitory in mature neurons, high intracellular chloride (due to low KCC2 expression) leads to an outward chloride and inward calcium current, resulting in depolarization. Importantly, these changes in KCC2 expression and GABA signaling have been noted in many neurological disorders (*e.g.* status epilepticus, spinal cord injury, TBI) (Plotkin et al., 1997, Bonislowski et al., 2007, Silayeva et al., 2015). The downregulation of KCC2 is associated with both calcium and chloride dyshomeostasis and cell death after ischemic stroke (Pond et al., 2004). Here, we observed elevated ipsilateral calcium and chloride levels, suggesting that similar KCC2 reductions occur after ICH. In general, while KCC2 receptors are downregulated after axonal injury, NKCC1 receptors may be unaffected or upregulated (Shulga et al., 2008, Cote et al., 2014). Thus, the PHZ chloride dyshomeostasis we observe after ICH may be primarily attributed to changes in KCC2 expression and intracellular chloride accumulation; a finding we believe warrants further investigation.

We found that BBB permeability, as measured by Gd concentration, was significantly correlated with K in the PHZ. Furthermore, we found that K⁺ concentrations are locally decreased after ICH and normalize with distance into the PHZ. This association is likely mediated by alterations in astrocytes after ICH. Astrocytes are a key component of the NVU/BBB and play an important role in regulating extracellular ion and neurotransmitter concentrations. In particular, astrocytes are important for maintenance of K⁺ homeostasis and express many K⁺ channels. When neurons release K⁺ following an action potential, astrocytes take up excess extracellular K⁺ and release it at its distal end, a process known as *K⁺ spatial buffering* (Gardner-Medwin, 1983, Kofuji and Newman, 2004). Alternatively, excess extracellular K⁺ and Cl⁻ can be stored in astrocytes, although this can contribute to edema (Walz, 2000). After ICH, astrocytes are activated in the PHZ within 72 hours, with elevated astrocyte numbers persisting to at least day 14 (Wang and Dore, 2008, Caliaperumal and Colbourne, 2014). Interestingly, astrocyte activation decreases from the hematoma edge into the PHZ (Wang, 2010). Here, we report that K⁺ is decreased in the PHZ and normalizes with distance from the hematoma 72 hours post-ICH; others report a similar pattern at Day 14 (Williamson et al., 2017). Considering the role astrocytes play in regulating potassium homeostasis, it is possible that the elevation in astrocyte numbers contributes to the observed decrease in PHZ potassium concentrations through increased spatial buffering.

As expected, iron dyshomeostasis was noted. Others have found PHZ iron accumulation at 24 hours post-ICH using a similar method (Auriat et al., 2012) and with more traditional methods (*i.e.* Perls stain) (Wu et al., 2011). In patients and in animal models, iron toxicity negatively contributes to functional outcome (Perez de la Ossa et al., 2010, Wu et al., 2011).

Iron accumulation after ICH is primarily a result of erythrocyte lysis. Erythrocyte lysis begins approximately one day after ICH, leading to Hb release (Wagner et al., 2003, Dang et al., 2017). Hb can then spontaneously oxidize, producing ferric heme and superoxide (Chen-Roetling et al., 2015). Heme breakdown by HO-1 produces iron, along with other metabolites (Xiong et al., 2014). Iron injection alone causes DNA damage, suggesting that iron contributes largely to oxidative stress following ICH (Nakamura et al., 2006). Furthermore, iron toxicity contributes to behavioral deficits, tissue loss, and neuronal degeneration (Caliaperumal et al., 2013).

We noted a rim of high Fe concentration in the hematoma close to the PHZ border, which may be reflective of the inflammatory response. Inflammatory response begins almost immediately after ICH, and MM Φ levels in the PHZ peak 2-3 days after ICH (Chen et al., 2015). MM Φ express two receptors to remove iron-containing compounds from the hematoma: the CD163 receptor, which facilitates the phagocytosis of free hemoglobin and hemoglobin-haptoglobin complexes, and the CD36 receptor, which facilitates erythrocyte phagocytosis (Febbraio et al., 2001, Thomsen et al., 2013). MM Φ localize at the PHZ/hematoma edge within 3 days of ICH and infiltrate the hematoma with time (Liu et al., 2015, Cao et al., 2016). Therefore, the high concentrations of iron observed at the hematoma edge here may represent a summation of both iron in the hematoma itself and iron internalized by microglia/macrophages (*i.e.* that present in hemoglobin).

3.5 Limitations

This research was done in the rat collagenase model of ICH and thus may not accurately reflect the full diversity of human ICH. The collagenase model has ongoing bleeding, and therefore only accurately represents ~30% of clinical ICH in respect to its bleeding pattern (Xi et al., 2006). Furthermore, we are concerned that this model may have bleeding lasting longer than previously thought (*e.g.* 3 hours) or may have a high incidence of re-bleeds. For example, a recent study by our lab found 40% of animals treated with hypothermia had 4 times higher bleeds than untreated animals, suggesting that the model may have weakened vasculature (Wowk et al., 2016). As many ICH patients have cerebral microbleeds pre- and post-stroke, this may be a clinically relevant feature of the collagenase model (Greenberg et al., 1999, Greenberg et al., 2004). Despite these limitations, the collagenase model is preferred over the AWB model due to the pattern of BBB injury.

This work had other limitations. First, we only measured BBB permeability to large molecules (~55-60 kDa). Importantly, the BBB may open to large molecules while still restricting movement of small ions and vice versa, so there is the possibility that the temporal progression of BBB permeability to small molecules differs from what is described here (Kang et al., 2013). Second, XFI cannot be used to determine the chemical state of iron or whether the observed ion dyshomeostasis is intra- or extra-cellular. The Australian Synchrotron has fine spatial resolution capable of determining intra- and extra-cellular levels of elements, including sodium, and thus will be a valuable tool in the future. Moreover, we were unable to elucidate a causal relationship between BBB damage and ion dyshomeostasis. Finally, functional significance of the described changes was not assessed. Acute behavioral assessment (*i.e.* within 72 hours of

ICH) is difficult to do early and is often confounded by processes such as edema (MacLellan et al., 2012).

3.6 Future directions

Further work is needed to determine whether hyperpermeability stems from late angiogenesis or microbleeds. Angiogenesis can be assessed by immunolabelling samples with the new vessel marker CD31 (Lei et al., 2015). As EB extravasation can be assessed with fluorescence microscopy, angiogenesis and Evans Blue extravasation could be measured simultaneously. We are particularly interested in the issue of re-bleeding and/or microhemorrhages. As previously mentioned, warfarin use has an 80-fold increased risk of transforming asymptomatic microhemorrhages into symptomatic ICH (Leary and Saver, 2003, Lee et al., 2009). Therefore, future experiments will administer warfarin on day 3, when there was the highest incidence of hyperpermeability and measure blood volume. We will also assess the extent to which inflammation contributes to the observed iron elevation at the hematoma edge using Perls stain to identify the quantity of Perls-positive macrophages at the hematoma edge, in regions of the PHZ, and in the contralateral hemisphere.

As we were unable to measure sodium dyshomeostasis with XFI, future research will use ICPMS to measure sodium concentrations in relation to BBB dysfunction using the same methods described here. Once we more fully understand the nature of ion dyshomeostasis after ICH, we are interested in causally linking alterations in ion dyshomeostasis with functional outcome. We will begin this line of research by administering bumetanide, an NKCC1

antagonist, to rats when acute (*i.e.* within 3 days) or chronic (*i.e.* at 7 days) chloride dyshomeostasis occurs. We will then assess long-term recovery with behavioral testing and with electrophysiology to test PHZ neuronal function. These findings should also be assessed in the AWB model of ICH. Not only would this follow industry recommendations, it could also provide insight into the mechanisms of BBB injury (National Institute of Neurological Disorders and Stroke Workshop, 2005). As previously mentioned, there is little progressive BBB injury in this model (MacLellan et al., 2008). Therefore, it is unlikely that the same ionic imbalances and Gd extravasation would be observed. If that is the case, it could provide insight into why AWB animals exhibit faster recovery as compared to collagenase animals.

3.7 Conclusions

This thesis evaluated the nature of BBB dysfunction after experimental ICH by measuring the temporal progression of BBB permeability and relating it to ion dyshomeostasis in the acute phase following stroke. Our findings confirm previous research finding that BBB injury peaks within 3 – 4 days of ICH. However, we reported the novel finding that there is high variability in BBB injury resolution; thus, future research should elucidate the mechanisms underlying this phenomenon. Furthermore, we established novel methodology and demonstrated that acute ion dyshomeostasis and BBB dysfunction occur after ICH. Ion dyshomeostasis is likely associated with BBB injury in vulnerable tissue. Taken together, these findings detail BBB injury after stroke and may inform future translational research. Finally, we advocate for the use of XFI to image Gd to allow for detailed spatial mapping of BBB injury.

Bibliography

- Abbott NJ, Patabendige AA, Dolman DE, Yusof SR, Begley DJ (2010) Structure and function of the blood-brain barrier. *Neurobiol Dis* 37:13-25.
- Abbott NJ, Ronnback L, Hansson E (2006) Astrocyte-endothelial interactions at the blood-brain barrier. *Nat Rev Neurosci* 7:41-53.
- Abraham MK, Chang WW (2016) Subarachnoid Hemorrhage. *Emergency medicine clinics of North America* 34:901-916.
- Abraham NG, Kappas A (2008) Pharmacological and clinical aspects of heme oxygenase. *Pharmacol Rev* 60:79-127.
- Adeoye O, Broderick JP (2010) Advances in the management of intracerebral hemorrhage. *Nature reviews Neurology* 6:593-601.
- Aksoy D, Bammer R, Mlynash M, Venkatasubramanian C, Eyingorn I, Snider RW, Gupta SN, Narayana R, Fischbein N, Wijman CA (2013) Magnetic resonance imaging profile of blood-brain barrier injury in patients with acute intracerebral hemorrhage. *Journal of the American Heart Association* 2:e000161.
- Alayash AI (2006) Redox and Radical Reactions of Hemoglobin Solutions: Toxicities and Protective Strategies. In: *Blood Substitutes* (Winslow, R. M., ed), pp 197-205.
- Alvarez JI, Dodelet-Devillers A, Kebir H, Ifergan I, Fabre PJ, Terouz S, Sabbagh M, Wosik K, Bourbonniere L, Bernard M, van Horssen J, de Vries HE, Charron F, Prat A (2011) The Hedgehog pathway promotes blood-brain barrier integrity and CNS immune quiescence. *Science* 334:1727-1731.
- Andreone BJ, Lacoste B, Gu C (2015) Neuronal and vascular interactions. *Annu Rev Neurosci* 38:25-46.
- Appelboom G, Bruce SS, Hickman ZL, Zacharia BE, Carpenter AM, Vaughan KA, Duren A, Hwang RY, Piazza M, Lee K, Claassen J, Mayer S, Badjatia N, Connolly ES, Jr. (2013) Volume-dependent effect of perihematomal oedema on outcome for spontaneous intracerebral haemorrhages. *J Neurol Neurosurg Psychiatry* 84:488-493.
- Arai K, Jin G, Navaratna D, Lo EH (2009) Brain angiogenesis in developmental and pathological processes: neurovascular injury and angiogenic recovery after stroke. *The FEBS journal* 276:4644-4652.
- Armulik A, Genove G, Mae M, Nisancioglu MH, Wallgard E, Niaudet C, He L, Norlin J, Lindblom P, Strittmatter K, Johansson BR, Betsholtz C (2010) Pericytes regulate the blood-brain barrier. *Nature* 468:557-561.
- Aronowski J, Zhao X (2011) Molecular pathophysiology of cerebral hemorrhage: secondary brain injury. *Stroke* 42:1781-1786.
- Auriat AM, Silasi G, Wei Z, Paquette R, Paterson P, Nichol H, Colbourne F (2012) Ferric iron chelation lowers brain iron levels after intracerebral hemorrhage in rats but does not improve outcome. *Exp Neurol* 234:136-143.
- Balami JS, Buchan AM (2012) Complications of intracerebral haemorrhage. *Lancet Neurol* 11:101-118.
- Balami JS, Chen RL, Grunwald IQ, Buchan AM (2011) Neurological complications of acute ischaemic stroke. *Lancet Neurol* 10:357-371.
- Bell RD, Winkler EA, Sagare AP, Singh I, LaRue B, Deane R, Zlokovic BV (2010) Pericytes control key neurovascular functions and neuronal phenotype in the adult brain and during brain aging. *Neuron* 68:409-427.
- Bladin CF, Alexandrov AV, Bellavance A, Bornstein N, Chambers B, Cote R, Lebrun L, Pirisi A, Norris JW (2000) Seizures after stroke: a prospective multicenter study. *Archives of neurology* 57:1617-1622.
- Bogousslavsky J, Van Melle G, Regli F (1988) The Lausanne Stroke Registry: analysis of 1,000 consecutive patients with first stroke. *Stroke* 19:1083-1092.

- Bonislowski DP, Schwarzbach EP, Cohen AS (2007) Brain injury impairs dentate gyrus inhibitory efficacy. *Neurobiol Dis* 25:163-169.
- Broderick J, Connolly S, Feldmann E, Hanley D, Kase C, Krieger D, Mayberg M, Morgenstern L, Ogilvy CS, Vespa P, Zuccarello M (2007) Guidelines for the management of spontaneous intracerebral hemorrhage in adults: 2007 update: a guideline from the American Heart Association/American Stroke Association Stroke Council, High Blood Pressure Research Council, and the Quality of Care and Outcomes in Research Interdisciplinary Working Group. *Circulation* 116:e391-413.
- Broderick JP, Brott TG, Duldner JE, Tomsick T, Huster G (1993) Volume of intracerebral hemorrhage. A powerful and easy-to-use predictor of 30-day mortality. *Stroke* 24:987-993.
- Caliaperumal J, Brodie S, Ma Y, Colbourne F (2014) Thrombin Causes Neuronal Atrophy and Acute but not Chronic Cell Death. *Can J Neurol Sci* 41:714-720.
- Caliaperumal J, Colbourne F (2014) Rehabilitation improves behavioral recovery and lessens cell death without affecting iron, ferritin, transferrin, or inflammation after intracerebral hemorrhage in rats. *Neurorehabil Neural Repair* 28:395-404.
- Caliaperumal J, Wowk S, Jones S, Ma Y, Colbourne F (2013) Bipyridine, an Iron Chelator, Does Not Lessen Intracerebral Iron-Induced Damage or Improve Outcome After Intracerebral Hemorrhagic Stroke in Rats. *Translational Stroke Research* 4:719-728.
- Canadian Stroke Network (2011) Quality of Stroke Care in Canada.
- Cao S, Zheng M, Hua Y, Chen G, Keep RF, Xi G (2016) Hematoma Changes During Clot Resolution After Experimental Intracerebral Hemorrhage. *Stroke* 47:1626-1631.
- Carmichael ST (2012) Brain Excitability in Stroke: The Yin and Yang of Stroke Progression. *Archives of neurology* 69:161-167.
- Castellanos M, Sobrino T, Millan M, Garcia M, Arenillas J, Nombela F, Brea D, Perez de la Ossa N, Serena J, Vivancos J, Castillo J, Davalos A (2007) Serum cellular fibronectin and matrix metalloproteinase-9 as screening biomarkers for the prediction of parenchymal hematoma after thrombolytic therapy in acute ischemic stroke: a multicenter confirmatory study. *Stroke* 38:1855-1859.
- Castellazzi M, Tamborino C, De Santis G, Garofano F, Lupato A, Ramponi V, Trentini A, Casetta I, Bellini T, Fainardi E (2010) Timing of serum active MMP-9 and MMP-2 levels in acute and subacute phases after spontaneous intracerebral hemorrhage. *Acta Neurochir Suppl* 106:137-140.
- Chang JJ, Emanuel BA, Mack WJ, Tsigoulis G, Alexandrov AV (2014) Matrix Metalloproteinase-9: Dual Role and Temporal Profile in Intracerebral Hemorrhage. *Journal of Stroke and Cerebrovascular Diseases* 23:2498-2505.
- Charidimou A, Gang Q, Werring DJ (2012) Sporadic cerebral amyloid angiopathy revisited: recent insights into pathophysiology and clinical spectrum. *J Neurol Neurosurg Psychiatry* 83:124-137.
- Chen-Roetling J, Lu X, Regan RF (2015) Targeting heme oxygenase after intracerebral hemorrhage. *Ther Targets Neurol Dis* 2.
- Chen H, Sun D (2005) The role of Na-K-Cl co-transporter in cerebral ischemia. *Neurological research* 27:280-286.
- Chen S, Yang QW, Chen G, Zhang JH (2015) An Update on Inflammation in the Acute Phase of Intracerebral Hemorrhage. *Translational Stroke Research* 6:4-8.
- Cote MP, Gandhi S, Zambrotta M, Houle JD (2014) Exercise modulates chloride homeostasis after spinal cord injury. *J Neurosci* 34:8976-8987.
- Daneman R, Zhou L, Kebede AA, Barres BA (2010) Pericytes are required for blood-brain barrier integrity during embryogenesis. *Nature* 468:562-566.
- Dang G, Yang Y, Wu G, Hua Y, Keep RF, Xi G (2017) Early Erytholysis in the Hematoma After Experimental Intracerebral Hemorrhage. *Transl Stroke Res* 8:174-182.

- David Y, Cacheaux LP, Ivens S, Lapilover E, Heinemann U, Kaufer D, Friedman A (2009) Astrocytic dysfunction in epileptogenesis: consequence of altered potassium and glutamate homeostasis? *J Neurosci* 29:10588-10599.
- De Herdt V, Dumont F, Henon H, Derambure P, Vonck K, Leys D, Cordonnier C (2011) Early seizures in intracerebral hemorrhage: incidence, associated factors, and outcome. *Neurology* 77:1794-1800.
- Delcourt C, Huang Y, Arima H, Chalmers J, Davis SM, Heeley EL, Wang J, Parsons MW, Liu G, Anderson CS (2012) Hematoma growth and outcomes in intracerebral hemorrhage: the INTERACT1 study. *Neurology* 79:314-319.
- Dohanish S, Goldstein H, Kofuncu E, Michel A, Pering C, Pietsch H, Schultze-Mosgau M, Steger-Hartmann T (2009) Overall risk assessment of Magnevist and other GBCAs in the context of Nephrogenic Systemic Fibrosis (NSF): Summary of possible risk factors and currently available scientific data. Bayer HealthCare Pharmaceuticals.
- Dowlatshahi D, Demchuk AM, Flaherty ML, Ali M, Lyden PL, Smith EE, On behalf of the VC (2011a) Defining hematoma expansion in intracerebral hemorrhage: Relationship with patient outcomes. *Neurology* 76:1238-1244.
- Dowlatshahi D, Smith EE, Flaherty ML, Ali M, Lyden P, Demchuk AM (2011b) Small intracerebral haemorrhages are associated with less haematoma expansion and better outcomes. *International journal of stroke : official journal of the International Stroke Society* 6:201-206.
- Duan X, Wen Z, Shen H, Shen M, Chen G (2016) Intracerebral Hemorrhage, Oxidative Stress, and Antioxidant Therapy. *Oxidative Medicine and Cellular Longevity* 2016:1203285.
- Dvorak HF, Brown LF, Detmar M, Dvorak AM (1995) Vascular permeability factor/vascular endothelial growth factor, microvascular hyperpermeability, and angiogenesis. *Am J Pathol* 146:1029-1039.
- Febbraio M, Hajjar DP, Silverstein RL (2001) CD36: a class B scavenger receptor involved in angiogenesis, atherosclerosis, inflammation, and lipid metabolism. *The Journal of clinical investigation* 108:785-791.
- Feigin VL, Krishnamurthi R, Bhattacherjee R, Parmar P, Theadom A, Hussein T, Purohit M, Hume P, Abbott M, Rush E, Kasabov N, Crezee I, Frielick S, Barker-Collo S, Barber PA, Arroll B, Poulton R, Ratnasabathy Y, Tobias M, Cabral N, Martins SC, Furtado LE, Lindsay P, Saposnik G, Giroud M, Bejot Y, Hacke W, Mehndiratta MM, Pandian JD, Gupta S, Padma V, Mandal DK, Kokubo Y, Ibrahim NM, Sahathevan R, Fu H, Wang W, Liu L, Hou ZG, Goncalves AF, Correia M, Varakin Y, Kravchenko M, Piradov M, Saadah M, Thrift AG, Cadilhac D, Davis S, Donnan G, Lopez AD, Hankey GJ, Maujean A, Kendall E, Brainin M, Abd-Allah F, Bornstein NM, Caso V, Marquez-Romero JM, Akinyemi RO, Bin Dhim NF, Norrving B, Sindi S, Kivipelto M, Mendis S, Ikram MA, Hofman A, Mirza SS, Rothwell PM, Sandercock P, Shakir R, Sacco RL, Culebras A, Roth GA, Moradi-Lakeh M, Murray C, Narayan KM, Mensah GA, Wiebers D, Moran AE, Group RSCW (2015) New strategy to reduce the global burden of stroke. *Stroke* 46:1740-1747.
- Felberg RA, Grotta JC, Shirzadi AL, Strong R, Narayana P, Hill-Felberg SJ, Aronowski J (2002) Cell death in experimental intracerebral hemorrhage: the "black hole" model of hemorrhagic damage. *Ann Neurol* 51:517-524.
- Fieschi C, Carolei A, Fiorelli M, Argentino C, Bozzao L, Fazio C, Salvetti M, Bastianello S (1988) Changing prognosis of primary intracerebral hemorrhage: results of a clinical and computed tomographic follow-up study of 104 patients. *Stroke* 19:192-195.
- Fiorelli M, Bastianello S, von Kummer R, del Zoppo GJ, Larrue V, Lesaffre E, Ringleb AP, Lorenzano S, Manelfe C, Bozzao L (1999) Hemorrhagic transformation within 36 hours of a cerebral infarct: relationships with early clinical deterioration and 3-month outcome in the European Cooperative Acute Stroke Study I (ECASS I) cohort. *Stroke* 30:2280-2284.

- Fisher CM (1971) Pathological observations in hypertensive cerebral hemorrhage. *J Neuropathol Exp Neurol* 30:536-550.
- Fisher CM (1972) Cerebral miliary aneurysms in hypertension. *Am J Pathol* 66:313-330.
- Fisher M (2008) Injuries to the vascular endothelium: vascular wall and endothelial dysfunction. *Rev Neurol Dis* 5 Suppl 1:S4-11.
- Flaherty ML, Woo D, Broderick JP (2010) The epidemiology of intracerebral hemorrhage. In: *Intracerebral Hemorrhage* (Carhuapoma, J. R. et al., eds): Cambridge University Press.
- Florczak-Rzepka M, Grond-Ginsbach C, Montaner J, Steiner T (2012) Matrix metalloproteinases in human spontaneous intracerebral hemorrhage: an update. *Cerebrovasc Dis* 34:249-262.
- Fraser PA (2011) The role of free radical generation in increasing cerebrovascular permeability. *Free Radic Biol Med* 51:967-977.
- Galeffi F, Sah R, Pond BB, George A, Schwartz-Bloom RD (2004) Changes in intracellular chloride after oxygen-glucose deprivation of the adult hippocampal slice: effect of diazepam. *J Neurosci* 24:4478-4488.
- Gamba G (2005) Molecular physiology and pathophysiology of electroneutral cation-chloride cotransporters. *Physiol Rev* 85:423-493.
- Gao F, Liu F, Chen Z, Hua Y, Keep RF, Xi G (2014) Hydrocephalus after intraventricular hemorrhage: the role of thrombin. *J Cereb Blood Flow Metab* 34:489-494.
- Gardner-Medwin AR (1983) A study of the mechanisms by which potassium moves through brain tissue in the rat. *The Journal of Physiology* 335:353-374.
- Gasche Y, Fujimura M, Morita-Fujimura Y, Copin JC, Kawase M, Massengale J, Chan PH (1999) Early appearance of activated matrix metalloproteinase-9 after focal cerebral ischemia in mice: a possible role in blood-brain barrier dysfunction. *J Cereb Blood Flow Metab* 19:1020-1028.
- Gastaldo J, Bencokova Z, Massart C, Joubert A, Balosso J, Charvet AM, Foray N (2011) Specific molecular and cellular events induced by irradiated X-ray photoactivatable drugs raise the problem of co-toxicities: particular consequences for anti-cancer synchrotron therapy. *Journal of synchrotron radiation* 18:456-463.
- George SJ, Webb SM, Abraham JL, Cramer SP (2010) Synchrotron X-ray analyses demonstrate phosphate-bound gadolinium in skin in nephrogenic systemic fibrosis. *The British journal of dermatology* 163:1077-1081.
- Gidday JM, Gasche YG, Copin JC, Shah AR, Perez RS, Shapiro SD, Chan PH, Park TS (2005) Leukocyte-derived matrix metalloproteinase-9 mediates blood-brain barrier breakdown and is proinflammatory after transient focal cerebral ischemia. *Am J Physiol Heart Circ Physiol* 289:H558-568.
- Gong C, Hoff JT, Keep RF (2000) Acute inflammatory reaction following experimental intracerebral hemorrhage in rat. *Brain Res* 871:57-65.
- Gonzales NR (2013) Ongoing Clinical Trials in Intracerebral Hemorrhage. *Stroke* 44:S70-S73.
- Gould B, McCourt R, Gioia LC, Kate M, Hill MD, Asdaghi N, Dowlathahi D, Jeerakathil T, Coutts SB, Demchuk AM, Emery D, Shuaib A, Butcher K (2014) Acute Blood Pressure Reduction in Patients With Intracerebral Hemorrhage Does Not Result in Borderzone Region Hypoperfusion. *Stroke* 45:2894-2899.
- Greenberg SM, Eng JA, Ning M, Smith EE, Rosand J (2004) Hemorrhage burden predicts recurrent intracerebral hemorrhage after lobar hemorrhage. *Stroke* 35:1415-1420.
- Greenberg SM, O'Donnell HC, Schaefer PW, Kraft E (1999) MRI detection of new hemorrhages: Potential marker of progression in cerebral amyloid angiopathy. *Neurology* 53:1135.
- Hackett MJ, DeSouza M, Caine S, Bewer B, Nichol H, Paterson PG, Colbourne F (2015) A New Method To Image Heme-Fe, Total Fe, and Aggregated Protein Levels after Intracerebral Hemorrhage. vol. 6, pp 761-770.

- Halleivi H, Abraham AT, Barreto AD, Grotta JC, Savitz SI (2010) The spot sign in intracerebral hemorrhage: the importance of looking for contrast extravasation. *Cerebrovasc Dis* 29:217-220.
- Hartz AM, Bauer B, Soldner EL, Wolf A, Boy S, Backhaus R, Mihaljevic I, Bogdahn U, Klunemann HH, Schuierer G, Schlachetzki F (2012) Amyloid-beta contributes to blood-brain barrier leakage in transgenic human amyloid precursor protein mice and in humans with cerebral amyloid angiopathy. *Stroke* 43:514-523.
- Hawkins BT, Davis TP (2005) The blood-brain barrier/neurovascular unit in health and disease. *Pharmacol Rev* 57:173-185.
- Heart and Stroke Foundation of Canada (2015a) 2015 Report on the Health of Canadians.
- Heart and Stroke Foundation of Canada (2015b) Access to Stroke Care: The Critical First Hours.
- Hemphill JC, Greenberg SM, Anderson CS, Becker K, Bendok BR, Cushman M, Fung GL, Goldstein JN, Macdonald RL, Mitchell PH, Scott PA, Selim MH, Woo D (2015) Guidelines for the Management of Spontaneous Intracerebral Hemorrhage. A Guideline for Healthcare Professionals From the American Heart Association/American Stroke Association 46:2032-2060.
- Herweh C, Juttler E, Schellinger PD, Klotz E, Schramm P (2010) Perfusion CT in hyperacute cerebral hemorrhage within 3 hours after symptom onset: is there an early perihemorrhagic penumbra? *J Neuroimaging* 20:350-353.
- Hop JW, Rinkel GJE, Algra A, van Gijn J (1997) Case-Fatality Rates and Functional Outcome After Subarachnoid Hemorrhage. A Systematic Review 28:660-664.
- Howard G, Cushman M, Howard VJ, Kissela BM, Kleindorfer DO, Moy CS, Switzer J, Woo D (2013) Risk Factors for Intracerebral Hemorrhage: The REasons for Geographic And Racial Differences in Stroke (REGARDS) Study. *Stroke; a journal of cerebral circulation* 44:1282-1287.
- Hu X, Tao C, Gan Q, Zheng J, Li H, You C (2016) Oxidative Stress in Intracerebral Hemorrhage: Sources, Mechanisms, and Therapeutic Targets. *Oxidative Medicine and Cellular Longevity* 2016:3215391.
- Hua Y, Keep RF, Hoff JT, Xi G (2007) Brain injury after intracerebral hemorrhage: the role of thrombin and iron. *Stroke* 38:759-762.
- Hua Y, Wu J, Keep RF, Nakamura T, Hoff JT, Xi G (2006) Tumor Necrosis Factor- α Increases in the Brain after Intracerebral Hemorrhage and Thrombin Stimulation. *Neurosurgery* 58:542-550.
- Huang FP, Xi G, Keep RF, Hua Y, Nemoianu A, Hoff JT (2002) Brain edema after experimental intracerebral hemorrhage: role of hemoglobin degradation products. *J Neurosurg* 96:287-293.
- Jansen T, Hortmann M, Oelze M, Opitz B, Steven S, Schell R, Knorr M, Karbach S, Schuhmacher S, Wenzel P, Munzel T, Daiber A (2010) Conversion of biliverdin to bilirubin by biliverdin reductase contributes to endothelial cell protection by heme oxygenase-1-evidence for direct and indirect antioxidant actions of bilirubin. *J Mol Cell Cardiol* 49:186-195.
- Jauch EC, Saver JL, Adams HP, Jr., Bruno A, Connors JJ, Demaerschalk BM, Khatri P, McMullan PW, Jr., Qureshi AI, Rosenfield K, Scott PA, Summers DR, Wang DZ, Wintermark M, Yonas H, American Heart Association Stroke C, Council on Cardiovascular N, Council on Peripheral Vascular D, Council on Clinical C (2013) Guidelines for the early management of patients with acute ischemic stroke: a guideline for healthcare professionals from the American Heart Association/American Stroke Association. *Stroke* 44:870-947.
- Jickling GC, Liu D, Stamova B, Ander BP, Zhan X, Lu A, Sharp FR (2014) Hemorrhagic transformation after ischemic stroke in animals and humans. *J Cereb Blood Flow Metab* 34:185-199.
- John RF, Williamson MR, Dietrich K, Colbourne F (2015) Localized hypothermia aggravates bleeding in the collagenase model of intracerebral hemorrhage. *Therapeutic hypothermia and temperature management* 5:19-25.
- Jorgensen HS, Nakayama H, Raaschou HO, Olsen TS (1999) Stroke. Neurologic and functional recovery the Copenhagen Stroke Study. *Phys Med Rehabil Clin N Am* 10:887-906.

- Kang EJ, Major S, Jorks D, Reiffurth C, Offenhauser N, Friedman A, Dreier JP (2013) Blood-brain barrier opening to large molecules does not imply blood-brain barrier opening to small ions. *Neurobiol Dis* 52:204-218.
- Karuppagounder SS, Alim I, Khim SJ, Bourassa MW, Sleiman SF, John R, Thinnis CC, Yeh T-L, Demetriades M, Neitemeier S, Cruz D, Gazaryan I, Killilea DW, Morgenstern L, Xi G, Keep RF, Schallert T, Tappero RV, Zhong J, Cho S, Maxfield FR, Holman TR, Culmsee C, Fong G-H, Su Y, Ming G-I, Song H, Cave JW, Schofield CJ, Colbourne F, Coppola G, Ratan RR (2016) Therapeutic targeting of oxygen-sensing prolyl hydroxylases abrogates ATF4-dependent neuronal death and improves outcomes after brain hemorrhage in several rodent models. *Science translational medicine* 8:328ra329-328ra329.
- Kassner A, Merali Z (2015) Assessment of Blood-Brain Barrier Disruption in Stroke. *Stroke* 46:3310-3315.
- Kastrup A, Groschel K, Ringer TM, Redecker C, Cordesmeyer R, Witte OW, Terborg C (2008) Early disruption of the blood-brain barrier after thrombolytic therapy predicts hemorrhage in patients with acute stroke. *Stroke* 39:2385-2387.
- Kate MP, Hansen MB, Mouridsen K, Ostergaard L, Choi V, Gould BE, McCourt R, Hill MD, Demchuk AM, Coutts SB, Dowlatshahi D, Emery DJ, Buck BH, Butcher KS, Investigators I (2014) Blood pressure reduction does not reduce perihematoma oxygenation: a CT perfusion study. *J Cereb Blood Flow Metab* 34:81-86.
- Katrak PH, Black D, Peeva V (2009) Do stroke patients with intracerebral hemorrhage have a better functional outcome than patients with cerebral infarction? *PM & R : the journal of injury, function, and rehabilitation* 1:427-433.
- Katsu M, Niizuma K, Yoshioka H, Okami N, Sakata H, Chan PH (2010) Hemoglobin-induced oxidative stress contributes to matrix metalloproteinase activation and blood-brain barrier dysfunction in vivo. *J Cereb Blood Flow Metab* 30:1939-1950.
- Kawai N, Nakamura T, Nagao S (2006) Early hemostatic therapy using recombinant factor VIIa in a collagenase-induced intracerebral hemorrhage model in rats. *Acta Neurochir Suppl* 96:212-217.
- Keep RF, Zhou N, Xiang J, Andjelkovic AV, Hua Y, Xi G (2014) Vascular disruption and blood-brain barrier dysfunction in intracerebral hemorrhage. *Fluids and Barriers of the CNS* 11:18-18.
- Keep RFX, J.; Ennis, S.R.; Andjelkovic, A.; Hua, Y.; Xi, G.; Hoff, J.T. (2008) Blood-brain barrier function in intracerebral hemorrhage. *Acta Neurochir Suppl* 105:73-77.
- Kelly PJ, Furie KL, Shafiqat S, Rallis N, Chang Y, Stein J (2003) Functional recovery following rehabilitation after hemorrhagic and ischemic stroke. *Archives of physical medicine and rehabilitation* 84:968-972.
- Kidwell CS, Burgess R, Menon R, Warach S, Latour LL (2011) Hyperacute injury marker (HARM) in primary hemorrhage: A distinct form of CNS barrier disruption. *Neurology* 77:1725-1728.
- Kirkman MA, Allan SM, Parry-Jones AR (2011) Experimental intracerebral hemorrhage: avoiding pitfalls in translational research. *Journal of Cerebral Blood Flow & Metabolism* 31:2135-2151.
- Kitaoka T, Hua Y, Xi G, Hoff JT, Keep RF (2002) Delayed argatroban treatment reduces edema in a rat model of intracerebral hemorrhage. *Stroke* 33:3012-3018.
- Klahr AC, Dickson CT, Colbourne F (2015) Seizure Activity Occurs in the Collagenase but not the Blood Infusion Model of Striatal Hemorrhagic Stroke in Rats. *Transl Stroke Res* 6:29-38.
- Klahr AC, Dietrich K, Dickson CT, Colbourne F (2016) Prolonged Localized Mild Hypothermia Does Not Affect Seizure Activity After Intracerebral Hemorrhage in Rats. *Therapeutic hypothermia and temperature management* 6:40-47.
- Knight RA, Han Y, Nagaraja TN, Whitton P, Ding J, Chopp M, Seyfried DM (2008) Temporal MRI assessment of intracerebral hemorrhage in rats. *Stroke* 39:2596-2602.

- Knowland D, Arac A, Sekiguchi KJ, Hsu M, Lutz SE, Perrino J, Steinberg GK, Barres BA, Nimmerjahn A, Agalliu D (2014) Stepwise recruitment of transcellular and paracellular pathways underlies blood-brain barrier breakdown in stroke. *Neuron* 82:603-617.
- Ko SB, Choi HA, Lee K (2012) Clinical syndromes and management of intracerebral hemorrhage. *Current atherosclerosis reports* 14:307-313.
- Kofuji P, Newman EA (2004) POTASSIUM BUFFERING IN THE CENTRAL NERVOUS SYSTEM. *Neuroscience* 129:1045-1056.
- Krueger H, Koot J, Hall RE, O'Callaghan C, Bayley M, Corbett D (2015) Prevalence of Individuals Experiencing the Effects of Stroke in Canada: Trends and Projections. *Stroke* 46:2226-2231.
- Krupinski J, Kaluza J, Kumar P, Kumar S, Wang JM (1994) Role of angiogenesis in patients with cerebral ischemic stroke. *Stroke* 25:1794-1798.
- Kuklina EV, Tong X, George MG, Bansil P (2012) Epidemiology and prevention of stroke: a worldwide perspective. *Expert Rev Neurother* 12:199-208.
- Le Duc G, Corde S, Charvet A-M, Elleaume H, Farion R, Le Bas J-F, Estève F (2004) In vivo measurement of gadolinium concentration in a rat glioma model by monochromatic quantitative computed tomography: comparison between gadopentetate dimeglumine and gadobutrol. *Investigative Radiology* 39:385-393.
- Le Duc G, Corde S, Elleaume H, Esteve F, Charvet AM, Brochard T, Fiedler S, Collomb A, Le Bas JF (2000) Feasibility of synchrotron radiation computed tomography on rats bearing glioma after iodine or gadolinium injection. *Jeune Equipe RSRM-UJF. European radiology* 10:1487-1492.
- Leary MC, Saver JL (2003) Annual incidence of first silent stroke in the United States: a preliminary estimate. *Cerebrovasc Dis* 16:280-285.
- Lee JM, Zhai G, Liu Q, Gonzales ER, Yin K, Yan P, Hsu CY, Vo KD, Lin W (2007) Vascular permeability precedes spontaneous intracerebral hemorrhage in stroke-prone spontaneously hypertensive rats. *Stroke* 38:3289-3291.
- Lee KR, Kawai N, Kim S, Sagher O, Hoff JT (1997) Mechanisms of edema formation after intracerebral hemorrhage: effects of thrombin on cerebral blood flow, blood-brain barrier permeability, and cell survival in a rat model. *J Neurosurg* 86:272-278.
- Lee SH, Ryu WS, Roh JK (2009) Cerebral microbleeds are a risk factor for warfarin-related intracerebral hemorrhage. *Neurology* 72:171-176.
- Lee SW, Kim WJ, Choi YK, Song HS, Son MJ, Gelman IH, Kim YJ, Kim KW (2003) SSeCKS regulates angiogenesis and tight junction formation in blood-brain barrier. *Nat Med* 9:900-906.
- Lei C, Zhang S, Cao T, Tao W, Liu M, Wu B (2015) HMGB1 may act via RAGE to promote angiogenesis in the later phase after intracerebral hemorrhage. *Neuroscience* 295:39-47.
- Leigh R, Jen SS, Hillis AE, Krakauer JW, Barker PB (2014) Pretreatment blood-brain barrier damage and post-treatment intracranial hemorrhage in patients receiving intravenous tissue-type plasminogen activator. *Stroke* 45:2030-2035.
- Li N, Liu YF, Ma L, Worthmann H, Wang YL, Wang YJ, Gao YP, Raab P, Dengler R, Weissenborn K, Zhao XQ (2013) Association of molecular markers with perihematomal edema and clinical outcome in intracerebral hemorrhage. *Stroke* 44:658-663.
- Li Z, Zhao X, Wang Y, Wang C, Liu L, Shao X, Wang W, Pan Y, Wang C, Ji R, Zhang C, Jing J, Wang Y (2015) Association between seizures and outcomes among intracerebral hemorrhage patients: the China National Stroke Registry. *Journal of stroke and cerebrovascular diseases : the official journal of National Stroke Association* 24:455-464.
- Lim-Hing K, Rincon F (2017) Secondary Hematoma Expansion and Perihemorrhagic Edema after Intracerebral Hemorrhage: From Bench Work to Practical Aspects. *Frontiers in Neurology* 8:74.

- Lischper M, Beuck S, Thanabalasundaram G, Pieper C, Galla HJ (2010) Metalloproteinase mediated occludin cleavage in the cerebral microcapillary endothelium under pathological conditions. *Brain Res* 1326:114-127.
- Liu B, Hu B, Shao S, Wu W, Fan L, Bai G, Shang P, Wang X (2015) CD163/Hemoglobin Oxygenase-1 Pathway Regulates Inflammation in Hematoma Surrounding Tissues after Intracerebral Hemorrhage. *Journal of stroke and cerebrovascular diseases : the official journal of National Stroke Association* 24:2800-2809.
- Liu DZ, Ander BP, Xu H, Shen Y, Kaur P, Deng W, Sharp FR (2010) Blood-brain barrier breakdown and repair by Src after thrombin-induced injury. *Ann Neurol* 67:526-533.
- Liu J, Jin X, Liu KJ, Liu W (2012) Matrix metalloproteinase-2-mediated occludin degradation and caveolin-1-mediated claudin-5 redistribution contribute to blood-brain barrier damage in early ischemic stroke stage. *J Neurosci* 32:3044-3057.
- Liu N, Cadilhac DA, Andrew NE (2014) Randomized controlled trial of early rehabilitation after intracerebral hemorrhage stroke: difference in outcomes within 6 months of stroke. *Stroke* 45:3502-3507.
- Lu A, Tang Y, Ran R, Ardizzone TL, Wagner KR, Sharp FR (2006) Brain genomics of intracerebral hemorrhage. *J Cereb Blood Flow Metab* 26:230-252.
- Lyden PD, Shuaib A, Lees KR, Davalos A, Davis SM, Diener HC, Grotta JC, Ashwood TJ, Hardemark HG, Svensson HH, Rodichok L, Wasiewski WW, Ahlberg G (2007) Safety and tolerability of NXY-059 for acute intracerebral hemorrhage: the CHANT Trial. *Stroke* 38:2262-2269.
- MacLellan CL, Auriat AM, McGie SC, Yan RH, Huynh HD, De Butte MF, Colbourne F (2006a) Gauging recovery after hemorrhagic stroke in rats: implications for cytoprotection studies. *J Cereb Blood Flow Metab* 26:1031-1042.
- MacLellan CL, Davies LM, Fingas MS, Colbourne F (2006b) The influence of hypothermia on outcome after intracerebral hemorrhage in rats. *Stroke* 37:1266-1270.
- MacLellan CL, Paquette R, Colbourne F (2012) A critical appraisal of experimental intracerebral hemorrhage research. *J Cereb Blood Flow Metab* 32:612-627.
- MacLellan CL, Plummer N, Silasi G, Auriat AM, Colbourne F (2011) Rehabilitation promotes recovery after whole blood-induced intracerebral hemorrhage in rats. *Neurorehabil Neural Repair* 25:477-483.
- MacLellan CL, Silasi G, Poon CC, Edmundson CL, Buist R, Peeling J, Colbourne F (2008) Intracerebral hemorrhage models in rat: comparing collagenase to blood infusion. *J Cereb Blood Flow Metab* 28:516-525.
- Manaenko A, Chen H, Zhang JH, Tang J (2011) Comparison of different preclinical models of intracerebral hemorrhage. *Acta Neurochir Suppl* 111:9-14.
- Marini C, Totaro R, De Santis F, Ciancarelli I, Baldassarre M, Carolei A (2001) Stroke in young adults in the community-based L'Aquila registry: incidence and prognosis. *Stroke* 32:52-56.
- Masada T, Hua Y, Xi G, Yang GY, Hoff JT, Keep RF (2001) Attenuation of intracerebral hemorrhage and thrombin-induced brain edema by overexpression of interleukin-1 receptor antagonist. *J Neurosurg* 95:680-686.
- Mayer SA, Brun NC, Begtrup K, Broderick J, Davis S, Diringer MN, Skolnick BE, Steiner T (2008) Efficacy and safety of recombinant activated factor VII for acute intracerebral hemorrhage. *The New England journal of medicine* 358:2127-2137.
- McCourt R, Gould B, Kate M, Asdaghi N, Kosior JC, Coutts S, Hill MD, Demchuk A, Jeerakathil T, Emery D, Butcher KS (2015) Blood-brain barrier compromise does not predict perihematoma edema growth in intracerebral hemorrhage. *Stroke* 46:954-960.

- Meguro R, Asano Y, Odagiri S, Li C, Iwatsuki H, Shoumura K (2007) Nonheme-iron histochemistry for light and electron microscopy: a historical, theoretical and technical review. *Archives of histology and cytology* 70:1-19.
- Meldrum BS, Nilsson B (1976) Cerebral blood flow and metabolic rate early and late in prolonged epileptic seizures induced in rats by bicuculline. *Brain* 99:523-542.
- Mittmann N, Seung SJ, Hill MD, Phillips SJ, Hachinski V, Cote R, Buck BH, Mackey A, Gladstone DJ, Howse DC, Shuaib A, Sharma M (2012) Impact of disability status on ischemic stroke costs in Canada in the first year. *Can J Neurol Sci* 39:793-800.
- Moller T, Weinstein JR, Hanisch UK (2006) Activation of microglial cells by thrombin: past, present, and future. *Semin Thromb Hemost* 32 Suppl 1:69-76.
- Montagne A, Toga AW, Zlokovic BV (2016) Blood-brain Barrier Permeability and Gadolinium: Benefits and Potential Pitfalls in Research. *JAMA neurology* 73:13-14.
- Montaner J, Alvarez-Sabin J, Molina CA, Angles A, Abilleira S, Arenillas J, Monasterio J (2001) Matrix metalloproteinase expression is related to hemorrhagic transformation after cardioembolic stroke. *Stroke* 32:2762-2767.
- Montaner J, Molina CA, Monasterio J, Abilleira S, Arenillas JF, Ribo M, Quintana M, Alvarez-Sabin J (2003) Matrix metalloproteinase-9 pretreatment level predicts intracranial hemorrhagic complications after thrombolysis in human stroke. *Circulation* 107:598-603.
- Montezano AC, Tsiropoulou S, Dulak-Lis M, Harvey A, Camargo LDL, Touyz RM (2015) Redox signaling, Nox5 and vascular remodeling in hypertension. *Current Opinion in Nephrology and Hypertension* 24:425-433.
- Morotti A, Goldstein JN (2016) Diagnosis and Management of Acute Intracerebral Hemorrhage. *Emergency medicine clinics of North America* 34:883-899.
- Moxon-Emre I, Schlichter LC (2011) Neutrophil depletion reduces blood-brain barrier breakdown, axon injury, and inflammation after intracerebral hemorrhage. *J Neuropathol Exp Neurol* 70:218-235.
- Mukherjee D, Patil CG (2011) Epidemiology and the global burden of stroke. *World Neurosurg* 76:S85-90.
- Murai Y, Ikeda Y, Teramoto A, Tsuji Y (1998) Magnetic resonance imaging-documented extravasation as an indicator of acute hypertensive intracerebral hemorrhage. *J Neurosurg* 88:650-655.
- Murthy SB, Moradiya Y, Dawson J, Lees KR, Hanley DF, Ziai WC (2015) Perihematomal Edema and Functional Outcomes in Intracerebral Hemorrhage: Influence of Hematoma Volume and Location. *Stroke* 46:3088-3092.
- Nabekura J, Ueno T, Okabe A, Furuta A, Iwaki T, Shimizu-Okabe C, Fukuda A, Akaike N (2002) Reduction of KCC2 expression and GABAA receptor-mediated excitation after in vivo axonal injury. *J Neurosci* 22:4412-4417.
- Nadeau SE, Dobkin B, Wu SS, Pei Q, Duncan PW (2015) The effects of stroke type, locus, and extent on long-term outcome of gait rehabilitation: the LEAPS experience. *Neurorehabil Neural Repair*.
- Nakamura T, Keep RF, Hua Y, Nagao S, Hoff JT, Xi G (2006) Iron-induced oxidative brain injury after experimental intracerebral hemorrhage *Acta Neurochirurgica [Suppl]* 96:194-198.
- National Institute of Neurological Disorders and Stroke Workshop (2005) Priorities for clinical research in intracerebral hemorrhage: report from a National Institute of Neurological Disorders and Stroke workshop. *Stroke* 36:e23-41.
- Nguyen AP, Huynh HD, Sjovold SB, Colbourne F (2008) Progressive brain damage and alterations in dendritic arborization after collagenase-induced intracerebral hemorrhage in rats. *Curr Neurovasc Res* 5:171-177.
- O'Collins VE, Macleod MR, Donnan GA, Horky LL, van der Worp BH, Howells DW (2006) 1,026 experimental treatments in acute stroke. *Ann Neurol* 59:467-477.

- Patel TR, Schielke GP, Hoff JT, Keep RF, Lorriss Betz A (1999) Comparison of cerebral blood flow and injury following intracerebral and subdural hematoma in the rat. *Brain Res* 829:125-133.
- Perez de la Ossa N, Sobrino T, Silva Y, Blanco M, Millan M, Gomis M, Agulla J, Araya P, Reverte S, Serena J, Davalos A (2010) Iron-related brain damage in patients with intracerebral hemorrhage. *Stroke* 41:810-813.
- Petzold GC, Murthy VN (2011) Role of astrocytes in neurovascular coupling. *Neuron* 71:782-797.
- Plotkin MD, Snyder EY, Hebert SC, Delpire E (1997) Expression of the Na-K-2Cl cotransporter is developmentally regulated in postnatal rat brains: a possible mechanism underlying GABA's excitatory role in immature brain. *J Neurobiol* 33:781-795.
- Pond BB, Galeffi F, Ahrens R, Schwartz-Bloom RD (2004) Chloride transport inhibitors influence recovery from oxygen-glucose deprivation-induced cellular injury in adult hippocampus. *Neuropharmacology* 47:253-262.
- Poon MT, Bell SM, Al-Shahi Salman R (2015) Epidemiology of Intracerebral Haemorrhage. *Frontiers of neurology and neuroscience* 37:1-12.
- Power C, Henry S, Del Bigio MR, Larsen PH, Corbett D, Imai Y, Yong VW, Peeling J (2003) Intracerebral hemorrhage induces macrophage activation and matrix metalloproteinases. *Ann Neurol* 53:731-742.
- Prousek J (2007) Fenton chemistry in biology and medicine. *PURE AND APPLIED CHEMISTRY* 79:2325-2338.
- Pun PB, Lu J, Moochhala S (2009) Involvement of ROS in BBB dysfunction. *Free Radic Res* 43:348-364.
- Pushie MJ, Pickering IJ, Korbas M, Hackett MJ, George GN (2014) Elemental and Chemically Specific X-ray Fluorescence Imaging of Biological Systems. *Chemical Reviews* 114:8499-8541.
- Qureshi AI, Mendelow AD, Hanley DF (2009) Intracerebral haemorrhage. *Lancet (London, England)* 373:1632-1644.
- Radu M, Chernoff J (2013) An in vivo assay to test blood vessel permeability. *JoVE (Journal of Visualized Experiments)* e50062-e50062.
- Regan RF, Kumar N, Gao F, Guo Y (2002) Ferritin induction protects cortical astrocytes from heme-mediated oxidative injury. *Neuroscience* 113:985-994.
- Rosell A, Cuadrado E, Ortega-Aznar A, Hernandez-Guillamon M, Lo EH, Montaner J (2008) MMP-9-positive neutrophil infiltration is associated to blood-brain barrier breakdown and basal lamina type IV collagen degradation during hemorrhagic transformation after human ischemic stroke. *Stroke* 39:1121-1126.
- Rosenberg GA, Estrada E, Kelley RO, Kornfeld M (1993) Bacterial collagenase disrupts extracellular matrix and opens blood-brain barrier in rat. *Neurosci Lett* 160:117-119.
- Rosenberg GA, Kornfeld M, Estrada E, Kelley RO, Liotta LA, Stetler-Stevenson WG (1992) TIMP-2 reduces proteolytic opening of blood-brain barrier by type IV collagenase. *Brain Res* 576:203-207.
- Rossi C, De Herdt V, Dequatre-Ponchelle N, Henon H, Leys D, Cordonnier C (2013) Incidence and predictors of late seizures in intracerebral hemorrhages. *Stroke* 44:1723-1725.
- Rossler K, Neuchrist C, Kitz K, Scheiner O, Kraft D, Lassmann H (1992) Expression of leucocyte adhesion molecules at the human blood-brain barrier (BBB). *J Neurosci Res* 31:365-374.
- Sacco S, Marini C, Carolei A (2004) Medical treatment of intracerebral hemorrhage. *Neurol Sci* 25 Suppl 1:S6-9.
- Sacco S, Marini C, Toni D, Olivieri L, Carolei A (2009) Incidence and 10-year survival of intracerebral hemorrhage in a population-based registry. *Stroke* 40:394-399.
- Sacco S, Ornello R, Degan D, Tiseo C, Pistoia F, Carolei A (2016) Declining incidence of intracerebral hemorrhage over two decades in a population-based study. *Eur J Neurol* 23:1627-1634.

- Samarasekera N, Smith C, Al-Shahi Salman R (2012) The association between cerebral amyloid angiopathy and intracerebral haemorrhage: systematic review and meta-analysis. *J Neurol Neurosurg Psychiatry* 83:275-281.
- Sandoval KE, Witt KA (2008) Blood-brain barrier tight junction permeability and ischemic stroke. *Neurobiol Dis* 32:200-219.
- Saulle MF, Schambra HM (2016) Recovery and Rehabilitation after Intracerebral Hemorrhage. *Semin Neurol* 36:306-312.
- Scalzo F, Alger JR, Hu X, Saver JL, Dani KA, Muir KW, Demchuk AM, Coutts SB, Luby M, Warach S, Liebeskind DS (2013) Multi-center prediction of hemorrhagic transformation in acute ischemic stroke using permeability imaging features. *Magn Reson Imaging* 31:961-969.
- Schlunk F, Greenberg SM (2015) The Pathophysiology of Intracerebral Hemorrhage Formation and Expansion. *Transl Stroke Res* 6:257-263.
- Schmidt-Kastner R, Meller D, Bellander BM, Stromberg I, Olson L, Ingvar M (1993) A one-step immunohistochemical method for detection of blood-brain barrier disturbances for immunoglobulins in lesioned rat brain with special reference to false-positive labelling in immunohistochemistry. *Journal of neuroscience methods* 46:121-132.
- Schoknecht K, David Y, Heinemann U (2015) The blood-brain barrier-gatekeeper to neuronal homeostasis: clinical implications in the setting of stroke. *Seminars in cell & developmental biology* 38:35-42.
- Shang H, Yang D, Zhang W, Li T, Ren X, Wang X, Zhao W (2013) Time course of Keap1-Nrf2 pathway expression after experimental intracerebral haemorrhage: correlation with brain oedema and neurological deficit. *Free Radic Res* 47:368-375.
- Shulga A, Thomas-Crusells J, Sigl T, Blaesse A, Mestres P, Meyer M, Yan Q, Kaila K, Saarna M, Rivera C, Giehl KM (2008) Posttraumatic GABA(A)-mediated $[Ca^{2+}]_i$ increase is essential for the induction of brain-derived neurotrophic factor-dependent survival of mature central neurons. *J Neurosci* 28:6996-7005.
- Siegenthaler JA, Sohet F, Daneman R (2013) 'Sealing off the CNS': cellular and molecular regulation of blood-brain barrierogenesis. *Curr Opin Neurobiol* 23:1057-1064.
- Siesjo BK, Agardh CD, Bengtsson F (1989) Free radicals and brain damage. *Cerebrovasc Brain Metab Rev* 1:165-211.
- Silasi G, Klahr AC, Hackett MJ, Auriat AM, Nichol H, Colbourne F (2012) Prolonged therapeutic hypothermia does not adversely impact neuroplasticity after global ischemia in rats. *J Cereb Blood Flow Metab* 32:1525-1534.
- Silayeva L, Deeb TZ, Hines RM, Kelley MR, Munoz MB, Lee HH, Brandon NJ, Dunlop J, Maguire J, Davies PA, Moss SJ (2015) KCC2 activity is critical in limiting the onset and severity of status epilepticus. *Proc Natl Acad Sci U S A* 112:3523-3528.
- Sreekrishnan A, Dearborn JL, Greer DM, Shi FD, Hwang DY, Leasure AC, Zhou SE, Gilmore EJ, Matouk CC, Petersen NH, Sansing LH, Sheth KN (2016) Intracerebral Hemorrhage Location and Functional Outcomes of Patients: A Systematic Literature Review and Meta-Analysis. *Neurocritical care* 25:384-391.
- Stankiewicz J, Panter SS, Neema M, Arora A, Batt CE, Bakshi R (2007) Iron in chronic brain disorders: imaging and neurotherapeutic implications. *Neurotherapeutics* 4:371-386.
- Szpak GM, Lechowicz W, Lewandowska E, Bertrand E, Wierzba-Bobrowicz T, Dymecki J (1999) Border zone neovascularization in cerebral ischemic infarct. *Folia neuropathologica* 37:264-268.
- Tang T, Liu X-J, Zhang Z-Q, Zhou H-J, Luo J-K, Huang J-F, Yang Q-D, Li X-Q (2007) Cerebral angiogenesis after collagenase-induced intracerebral hemorrhage in rats. *Brain Research* 1175:134-142.
- Thomsen JH, Etzerodt A, Svendsen P, Moestrup SK (2013) The haptoglobin-CD163-heme oxygenase-1 pathway for hemoglobin scavenging. *Oxid Med Cell Longev* 2013:523652.

- Thurston G, Suri C, Smith K, McClain J, Sato TN, Yancopoulos GD, McDonald DM (1999) Leakage-resistant blood vessels in mice transgenically overexpressing angiopoietin-1. *Science* 286:2511-2514.
- Tian Y, Wang Z, Jia Y, Li S, Wang B, Wang S, Sun L, Zhang J, Chen J, Jiang R (2013) Intracranial pressure variability predicts short-term outcome after intracerebral hemorrhage: a retrospective study. *Journal of the neurological sciences* 330:38-44.
- Toth P, Tarantini S, Springo Z, Tucsek Z, Gautam T, Giles CB, Wren JD, Koller A, Sonntag WE, Csiszar A, Ungvari Z (2015) Aging exacerbates hypertension-induced cerebral microhemorrhages in mice: role of resveratrol treatment in vasoprotection. *Aging Cell* 14:400-408.
- Urday S, Beslow LA, Dai F, Zhang F, Battey TW, Vashkevich A, Ayres AM, Leasure AC, Selim MH, Simard JM, Rosand J, Kimberly WT, Sheth KN (2016) Rate of Perihematomal Edema Expansion Predicts Outcome After Intracerebral Hemorrhage. *Critical care medicine* 44:790-797.
- van Asch CJ, Luitse MJ, Rinkel GJ, van der Tweel I, Algra A, Klijn CJ (2010) Incidence, case fatality, and functional outcome of intracerebral haemorrhage over time, according to age, sex, and ethnic origin: a systematic review and meta-analysis. *Lancet Neurol* 9:167-176.
- Veikkola T, Alitalo K (1999) VEGFs, receptors and angiogenesis. *Seminars in cancer biology* 9:211-220.
- Venkatasubramanian C, Mlynash M, Finley-Caulfield A, Eyngorn I, Kalimuthu R, Snider RW, Wijman CA (2011) Natural history of perihematomal edema after intracerebral hemorrhage measured by serial magnetic resonance imaging. *Stroke* 42:73-80.
- Viswanathan A, Greenberg SM (2011) Cerebral amyloid angiopathy in the elderly. *Ann Neurol* 70:871-880.
- Wagner KR, Sharp FR, Ardizzone TD, Lu A, Clark JF (2003) Heme and iron metabolism: role in cerebral hemorrhage. *J Cereb Blood Flow Metab* 23:629-652.
- Wagner KR, Xi G, Hua Y, Kleinholz M, de Courten-Myers GM, Myers RE, Broderick JP, Brott TG (1996) Lobar intracerebral hemorrhage model in pigs: rapid edema development in perihematomal white matter. *Stroke* 27:490-497.
- Wagner KR, Xi G, Hua Y, Zuccarello M, de Courten-Myers GM, Broderick JP, Brott TG (1999) Ultra-early clot aspiration after lysis with tissue plasminogen activator in a porcine model of intracerebral hemorrhage: edema reduction and blood-brain barrier protection. *J Neurosurg* 90:491-498.
- Wagner KR, Zuccarello M (2009) Animal models and experimental treatments of intracerebral hemorrhage
- Intracerebral Hemorrhage. (Carhuapoma, J. R. et al., eds): Cambridge University Press.
- Walz W (2000) Role of astrocytes in the clearance of excess extracellular potassium. *Neurochem Int* 36:291-300.
- Wang G, Hu W, Tang Q, Wang L, Sun XG, Chen Y, Yin Y, Xue F, Sun Z (2016) Effect Comparison of Both Iron Chelators on Outcomes, Iron Deposit, and Iron Transporters After Intracerebral Hemorrhage in Rats. *Molecular neurobiology* 53:3576-3585.
- Wang G, Yang Q, Li G, Wang L, Hu W, Tang Q, Li D, Sun Z (2011) Time course of heme oxygenase-1 and oxidative stress after experimental intracerebral hemorrhage. *Acta Neurochir (Wien)* 153:319-325.
- Wang J (2010) Preclinical and clinical research on inflammation after intracerebral hemorrhage. *Progress in neurobiology* 92:463-477.
- Wang J, Dore S (2007) Inflammation after intracerebral hemorrhage. *J Cereb Blood Flow Metab* 27:894-908.
- Wang J, Dore S (2008) HEME OXYGENASE 2 DEFICIENCY INCREASES BRAIN SWELLING AND INFLAMMATION AFTER INTRACEREBRAL HEMORRHAGE. *Neuroscience* 155:1133-1141.

- Warkentin LM, Auriat AM, Wowk S, Colbourne F (2010) Failure of deferoxamine, an iron chelator, to improve outcome after collagenase-induced intracerebral hemorrhage in rats. *Brain Res* 1309:95-103.
- Wasserman JK, Schlichter LC (2007) Minocycline protects the blood-brain barrier and reduces edema following intracerebral hemorrhage in the rat. *Exp Neurol* 207:227-237.
- Williamson MR, Dietrich K, Hackett MJ, Caine S, Nadeau CA, Aziz JR, Nichol H, Paterson PG, Colbourne F (2017) Rehabilitation Augments Hematoma Clearance and Attenuates Oxidative Injury and Ion Dyshomeostasis After Brain Hemorrhage. *Stroke* 48:195-203.
- World Health Organization (2008) *The Global Burden of Disease: 2004 Update*.
- Wosik K, Cayrol R, Dodelet-Devillers A, Berthelet F, Bernard M, Moumdjian R, Bouthillier A, Reudelhuber TL, Prat A (2007) Angiotensin II controls occludin function and is required for blood brain barrier maintenance: relevance to multiple sclerosis. *J Neurosci* 27:9032-9042.
- Wowk S, Fagan KJ, Ma Y, Nichol H, Colbourne F (2016) Examining potential side effects of therapeutic hypothermia in experimental intracerebral hemorrhage. *J Cereb Blood Flow Metab* 271678x16681312.
- Wowk S, Ma Y, Colbourne F (2014) Mild therapeutic hypothermia does not reduce thrombin-induced brain injury. *Therapeutic hypothermia and temperature management* 4:180-187.
- Wu G, Xi G, Huang F (2006) Spontaneous intracerebral hemorrhage in humans: hematoma enlargement, clot lysis, and brain edema. *Acta Neurochir Suppl* 96:78-80.
- Wu H, Wu T, Xu X, Wang J, Wang J (2011) Iron toxicity in mice with collagenase-induced intracerebral hemorrhage. *J Cereb Blood Flow Metab* 31:1243-1250.
- Wu H, Zhang Z, Li Y, Zhao R, Li H, Song Y, Qi J, Wang J (2010) Time course of upregulation of inflammatory mediators in the hemorrhagic brain in rats: correlation with brain edema. *Neurochemistry international* 57:248-253.
- Wu J, Hua Y, Keep RF, Nakamura T, Hoff JT, Xi G (2003) Iron and iron-handling proteins in the brain after intracerebral hemorrhage. *Stroke* 34:2964-2969.
- Wu J, Hua Y, Keep RF, Schallert T, Hoff JT, Xi G (2002) Oxidative brain injury from extravasated erythrocytes after intracerebral hemorrhage. *Brain Res* 953:45-52.
- Xi G, Hua Y, Bhasin RR, Ennis SR, Keep RF, Hoff JT (2001) Mechanisms of edema formation after intracerebral hemorrhage: effects of extravasated red blood cells on blood flow and blood-brain barrier integrity. *Stroke* 32:2932-2938.
- Xi G, Keep RF, Hoff JT (2006) Mechanisms of brain injury after intracerebral haemorrhage. *Lancet Neurol* 5:53-63.
- Xiong XY, Wang J, Qian ZM, Yang QW (2014) Iron and intracerebral hemorrhage: from mechanism to translation. *Transl Stroke Res* 5:429-441.
- Xu J, Qiu GP, Huang J, Zhang B, Sun SQ, Gan SW, Lu WT, Wang KJ, Huang SQ, Zhu SJ (2015) Internalization of aquaporin-4 after collagenase-induced intracerebral hemorrhage. *Anatomical record (Hoboken, NJ : 2007)* 298:554-561.
- Xue M, Del Bigio MR (2000) Intracerebral injection of autologous whole blood in rats: time course of inflammation and cell death. *Neurosci Lett* 283:230-232.
- Xue M, Del Bigio MR (2003) Comparison of brain cell death and inflammatory reaction in three models of intracerebral hemorrhage in adult rats. *Journal of stroke and cerebrovascular diseases : the official journal of National Stroke Association* 12:152-159.
- Yan T, Chopp M, Chen J (2015) Experimental animal models and inflammatory cellular changes in cerebral ischemic and hemorrhagic stroke. *Neurosci Bull* 31:717-734.
- Yang GY, Betz AL, Chenevert TL, Brunberg JA, Hoff JT (1994) Experimental intracerebral hemorrhage: relationship between brain edema, blood flow, and blood-brain barrier permeability in rats. *J Neurosurg* 81:93-102.

- Yang J, Arima H, Wu G, Heeley E, Delcourt C, Zhou J, Chen G, Wang X, Zhang S, Yu S, Chalmers J, Anderson CS (2015) Prognostic significance of perihematomal edema in acute intracerebral hemorrhage: pooled analysis from the intensive blood pressure reduction in acute cerebral hemorrhage trial studies. *Stroke* (00392499) 46:1009-1013 1005p.
- Yang S, Chen Y, Deng X, Jiang W, Li B, Fu Z, Du M, Ding R (2013) Hemoglobin-induced nitric oxide synthase overexpression and nitric oxide production contribute to blood-brain barrier disruption in the rat. *J Mol Neurosci* 51:352-363.
- Yang Y, Estrada EY, Thompson JF, Liu W, Rosenberg GA (2007) Matrix metalloproteinase-mediated disruption of tight junction proteins in cerebral vessels is reversed by synthetic matrix metalloproteinase inhibitor in focal ischemia in rat. *J Cereb Blood Flow Metab* 27:697-709.
- Yang Y, Rosenberg GA (2011) MMP-mediated disruption of claudin-5 in the blood-brain barrier of rat brain after cerebral ischemia. *Methods Mol Biol* 762:333-345.
- Yeatts SD, Palesch YY, Moy CS, Selim M (2013) High dose deferoxamine in intracerebral hemorrhage (HI-DEF) trial: rationale, design, and methods. *Neurocritical care* 19:257-266.
- Zazulia AR, Diringner MN, Derdeyn CP, Powers WJ (1999) Progression of mass effect after intracerebral hemorrhage. *Stroke* 30:1167-1173.
- Zazulia AR, Diringner MN, Videen TO, Adams RE, Yundt K, Aiyagari V, Grubb RL, Jr., Powers WJ (2001) Hypoperfusion without ischemia surrounding acute intracerebral hemorrhage. *J Cereb Blood Flow Metab* 21:804-810.
- Zhang ZG, Zhang L, Tsang W, Soltanian-Zadeh H, Morris D, Zhang R, Goussev A, Powers C, Yeich T, Chopp M (2002) Correlation of VEGF and angiopoietin expression with disruption of blood-brain barrier and angiogenesis after focal cerebral ischemia. *J Cereb Blood Flow Metab* 22:379-392.
- Zhao F, Hua Y, He Y, Keep RF, Xi G (2011) Minocycline-induced attenuation of iron overload and brain injury after experimental intracerebral hemorrhage. *Stroke* 42:3587-3593.
- Zhao X, Sun G, Zhang J, Strong R, Dash PK, Kan YW, Grotta JC, Aronowski J (2007) Transcription factor Nrf2 protects the brain from damage produced by intracerebral hemorrhage. *Stroke* 38:3280-3286.
- Zheng W, Haacke EM, Webb SM, Nichol H (2012) Imaging of stroke: a comparison between X-ray fluorescence and magnetic resonance imaging methods. *Magnetic resonance imaging* 30:10.1016/j.mri.2012.1004.1011.
- Zhou Y, Wang Y, Wang J, Anne Stetler R, Yang QW (2014) Inflammation in intracerebral hemorrhage: from mechanisms to clinical translation. *Prog Neurobiol* 115:25-44.
- Zille M, Karuppagounder SS, Chen Y, Gough PJ, Bertin J, Finger J, Milner TA, Jonas EA, Ratan RR (2017) Neuronal Death After Hemorrhagic Stroke In Vitro and In Vivo Shares Features of Ferroptosis and Necroptosis. *Stroke* 48:1033-1043.

TABLES

Table 1-1. Comparison of the two most commonly used intracerebral hemorrhage models, including model characteristics and clinical relevance.

| Autologous whole blood model | Collagenase model |
|---|--|
| Characteristics* | |
| Less neutrophil infiltration | Greater neutrophil infiltration |
| Less tissue loss | Greater tissue loss |
| Less extensive white matter damage | More extensive white matter damage |
| Less severe functional deficits; faster recovery | More severe and longer-lasting functional deficits |
| Less edema | Greater edema |
| Clinical relevance** | |
| Does not mimic spontaneous vessel rupture | Mimics spontaneous vessel rupture |
| No hematoma expansion – relevant for ~70% of patients | Hematoma expansion – relevant for ~30% of patients |
| Edema onset is faster and resolved more quickly | Edema onset is faster and resolved more quickly |
| Poor relevance for modeling deficits | Greater relevance for modeling functional deficits in patients |
| Elevated inflammatory response | Elevated inflammatory response |

*as compared to the other model

**as compared to clinical populations

Table 2-1. Relationship (Pearson’s rho) between Gd concentration and Ca, Cu, Cl, Fe, K, Mn, and Zn concentration in the hematoma and perihematoma zone at day 3 post-ICH. Bolded *p*-values indicate $p < 0.05$.

| | Hematoma | | Perihematoma Zone | |
|----|----------|--------------|-------------------|--------------|
| | r | p value | r | p value |
| Ca | 0.731 | 0.160 | N/A | N/A |
| Cu | 0.811 | 0.096 | N/A | N/A |
| Cl | 0.575 | 0.311 | 0.541 | 0.134 |
| Fe | 0.663 | 0.223 | -0.412 | 0.494 |
| K | 0.644 | 0.241 | 0.849 | 0.049 |
| Mn | 0.989 | 0.001 | N/A | N/A |
| Zn | 0.606 | 0.279 | N/A | N/A |

Table 2-2. Relationship (Pearson’s rho) between Gd concentration and Fe, Cl, and K concentration every 180 μm into the perihematoma zone at day 3 post-ICH. Bolded p -values indicate $p < 0.05$.

| Distance | Fe | | Cl | | K | |
|-------------|--------|-------|-------|--------------|-------|--------------|
| | r | P | r | p | r | p |
| 0 – 180 | -0.318 | 0.249 | 0.108 | 0.701 | 0.419 | 0.200 |
| 181 – 360 | -0.086 | 0.760 | 0.358 | 0.191 | 0.294 | 0.287 |
| 361 – 540 | -0.284 | 0.301 | 0.454 | 0.089 | 0.528 | 0.043 |
| 541 – 720 | -0.277 | 0.318 | 0.334 | 0.224 | 0.460 | 0.084 |
| 721 – 900 | -0.161 | 0.567 | 0.401 | 0.139 | 0.499 | 0.058 |
| 901 – 1080 | -0.153 | 0.587 | 0.611 | 0.016 | 0.565 | 0.028 |
| 1081 – 1260 | -0.499 | 0.058 | 0.619 | 0.014 | 0.595 | 0.019 |

FIGURES

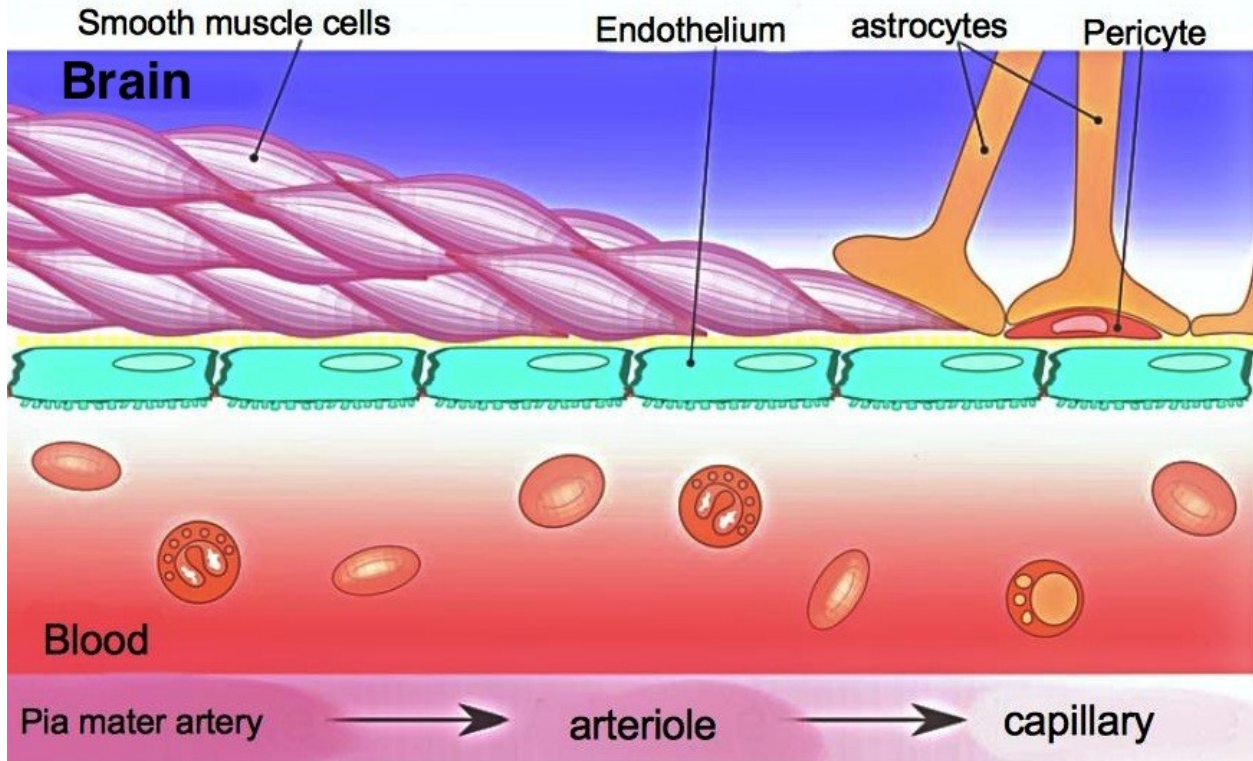


Figure 1-1. Blood-brain barrier structure. From Armin Kübelbeck (https://commons.wikimedia.org/wiki/File:Blood_vessels_brain_english.jpg), "Blood vessels brain English", <https://creativecommons.org/licenses/by/3.0/legalcode>.

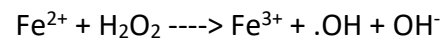


Figure 1-2. Fenton's Reaction.

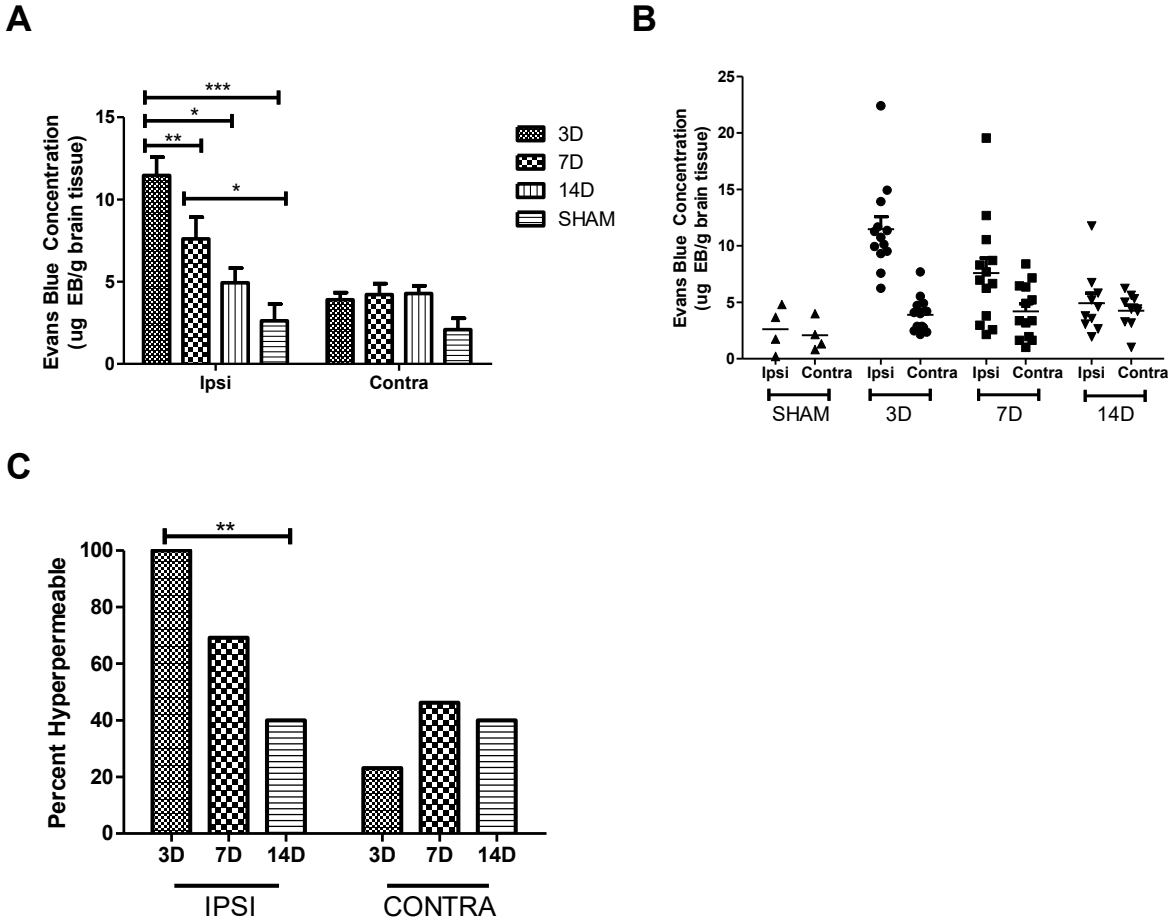


Figure 2-1. Evans Blue extravasation at day 3 was significantly higher than days 7, 14, and SHAM in the IPSI hemisphere. Significant elevations persisted to day 7. There were no differences in Evans Blue extravasation in the CONTRA hemisphere (A). High variability was observed at all times measured (B). A chi-squared test revealed a significant relationship between BBB dysfunction incidence and time in the IPSI, but not CONTRA, hemisphere (C). * $P < 0.05$ ** $P < 0.01$ *** $P < 0.001$.

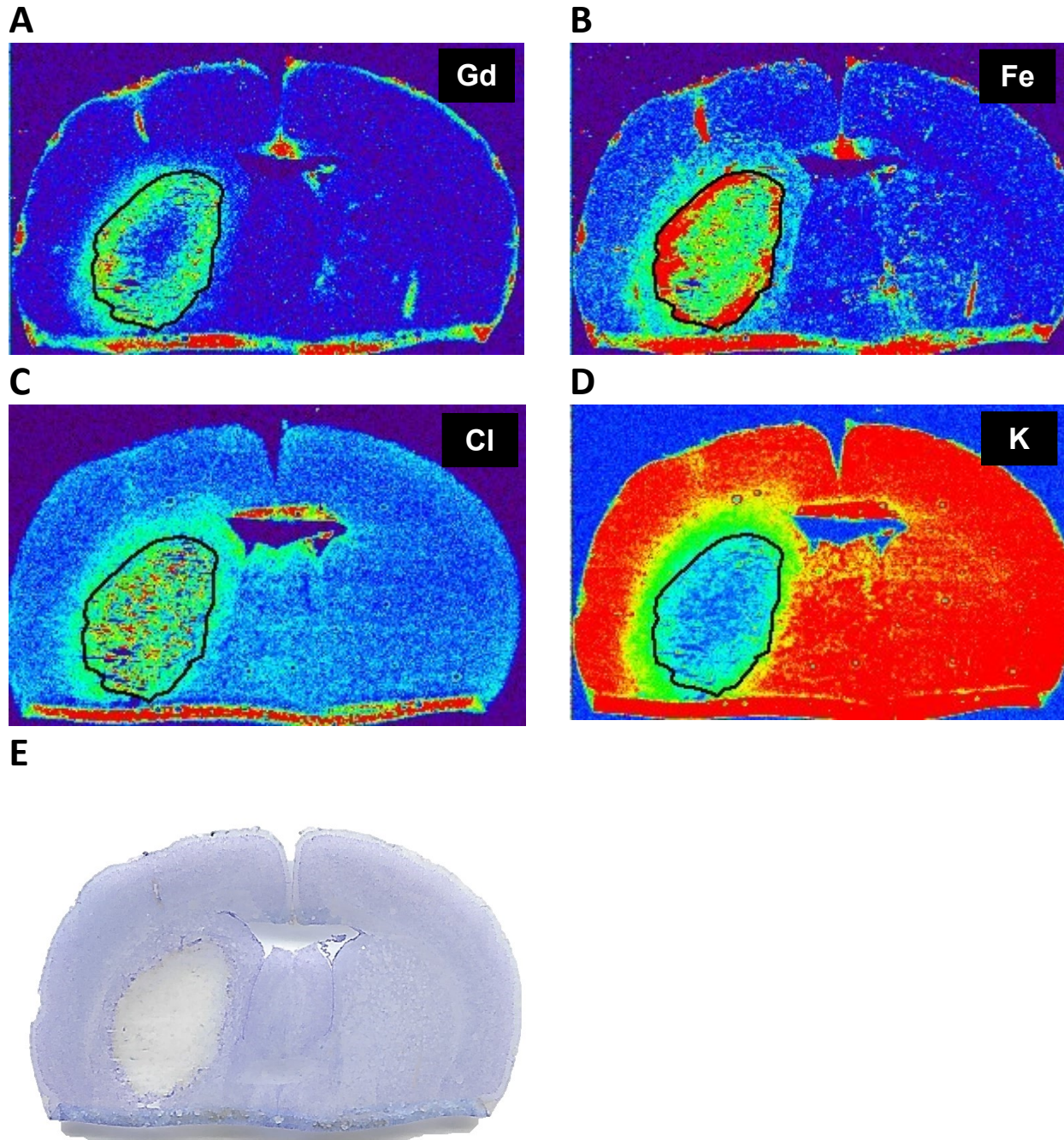


Figure 2-2. Representative images comparing X-ray fluorescence imaging of Gd (A) Fe (B), Cl (C) and K (D). The black line marks the hematoma boundary. Diffusion of ion dyshomeostasis and BBB permeability are more easily assessed using X-ray fluorescence imaging than cresyl violet staining (E). Cresyl violet staining confirms the hematoma boundaries determined with XFI. Tissue in the hematoma is more fragile and appears to have been damaged/destroyed in the staining process (E).

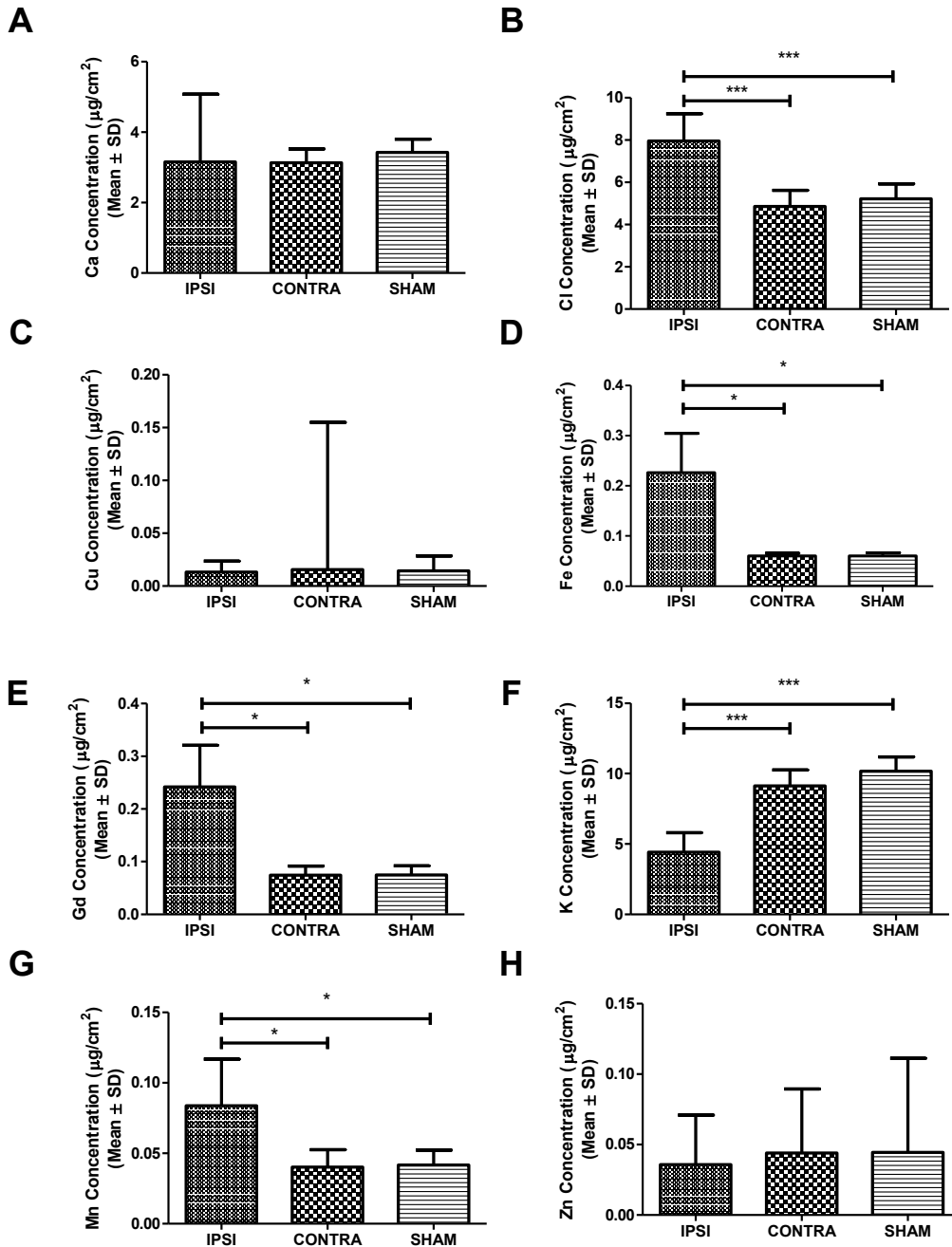


Figure 2-3. X-ray fluorescence analysis reveals that Ca, Cu, and Zn in the hematoma are unaffected by intracerebral hemorrhage at day 3 post-injury (A, C, H). Cl, Fe, Gd, and Mn concentrations in the IPSI hematoma were significantly increased as compared to CONTRA and SHAM hemispheres (B, D, E, G). K concentrations were significantly decreased in the IPSI hematoma as compared to CONTRA and SHAM hemispheres (F). * $P < 0.05$ ** $P < 0.01$ *** $P < 0.001$.

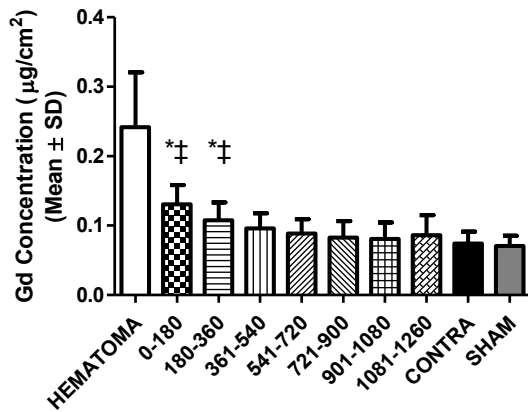
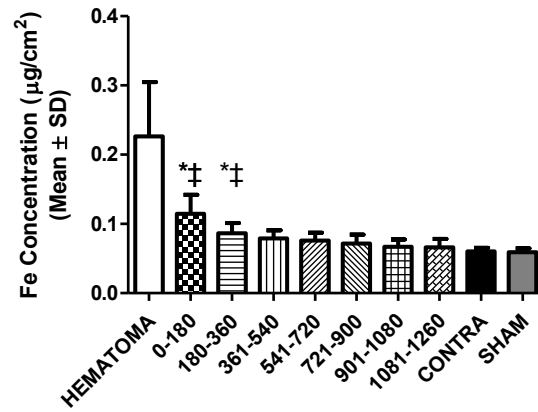
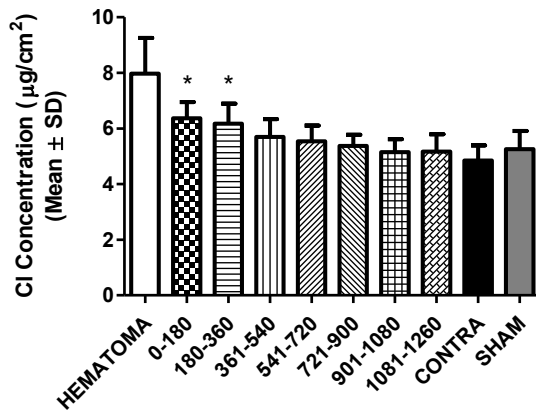
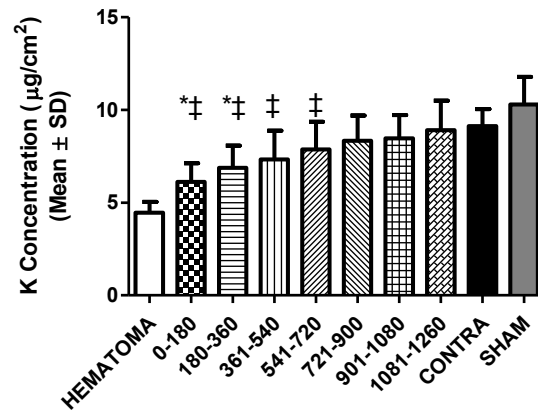
A**B****C****D**

Figure 2-4. There was a distance main effect for Gd, Fe, and Cl, such that values were highest in the hematoma and decreased with distance into the perihematoma zone (A-C). There was a distance main effect for K, where values were lowest in the hematoma and normalized with distance into the perihematoma zone (D). * $P < 0.05$ as compared to CONTRA. ‡ $P < 0.05$ as compared to SHAM. Hematoma is shown for reference but was excluded from the analyses.

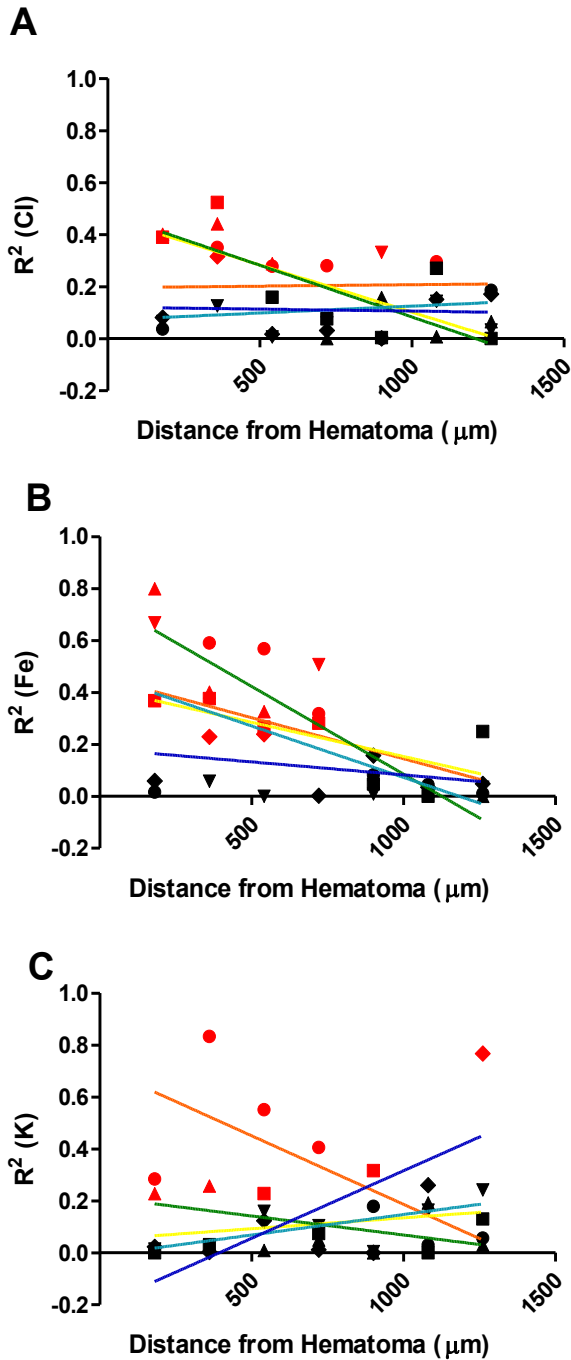


Figure 2-5. The proportion of Cl and K variance accounted for by Gd concentration does not change with distance from the hematoma edge for most animals (A, C). Gd concentration can strongly predict Fe concentration close to the hematoma/PHZ interface. This effect disappears with distance into the PHZ (B). Each regression line represents a single sample. Red data points indicate a significant correlation.